NASA Contractor Report 165852

Transonic Perturbation Analysis of Wing-Fuselage-Nacelle-Pylon Configurations with Powered Jet Exhausts

J.C. Wai, C.C. Sun, and H. Yoshihara

BOEING MILITARY AIRPLANE COMPANY
Seattle, WA 98124

Contract NAS1-15887
February 1982

National Aeronautics and Space Administration

Langley Research Center
Hampton, Virginia 23665

NASA Contractor Report 165852

Transonic Perturbation Analysis of Wing-Fuselage-Nacelle-Pylon Configurations with Powered Jet Exhausts

J.C. Wai, C.C. Sun, and H. Yoshihara

BOEING MILITARY AIRPLANE COMPANY
Seattle, WA 98124

Contract NAS1-15887
February 1982

National Aeronautics and Space Administration

Langley Research Center
Hampton, Virginia 23665

SUMMARY

A method using a transonic small disturbance code with successive line over-relaxation (SLOR) is described for treating wing/fuselage configurations with a nacelle/pylon/powered jet. Examples illustrating its use for the NASA transport research model are given. Reasonable test/theory comparisons were obtained.

TABLE OF CONTENTS

LIST OF SYMBOLS

b	Wing span
C	Constant of integration (Eq. 7)
c	Local chord
C_D	Drag coefficient
C_L	Lift coefficient
C_p	Pressure Coefficient
C_p^*	Sonic pressure coefficient
F	Function describing the configuration
J	Function defining jet boundary
M	Mach No.
p	Pressure
t	Wing thickness
V	Reference velocity
x,y,z	Cartesian coordinates
α	Angle of attack
Δ	Increment
γ	Ratio of specific heats

η	Normalized spanwise coordinate
ξ	Normalized chordwise coordinate
ϕ	Perturbation potential

SUBSCRIPT

∞	Free stream
j	Jet

INTRODUCTION

Engine installations on the wing upper surface experience severe adverse interference in the transonic regime when the nacelle, pylon, and jet exhaust plume are immersed in the supersonic region of the wing flow field. Significant adverse interference can also arise in underwing installations of large diameter high bypass ratio engines. This interference arises when local supersonic regions and shock waves occur due to the close proximity of the nacelles to the wing required by landing gear length or center of gravity considerations.

Transonic computer programs to handle wing/nacelle/pylon configurations have been developed, for example, by Boppe (Ref. 1) and more recently by Yu (Ref. 2). Boppe's method is based on the small disturbance approximation. It utilizes an embedded grid system in which a highly refined cartesian grid surrounds each configuration component. The fluid dynamic coupling between the fine grids is accomplished via a coarse background grid. The superfine local grids are intended to moderate the difficulties of fulfilling boundary conditions with a mesh non-conformal to the configuration. Boppe's method can only handle the flow-through nacelle cases; therefore, no special consideration is required at the jet exhaust boundary, since the flow there is continuous.

Yu's method is based on the exact potential equation and employs the finite volume algorithm developed by Jameson and Caughey (Ref. 3). The mesh is conformal to the wing/fuselage, and the nacelle/pylon tangency condition is imposed by means of transpiration velocities. The jet exhaust plume is modeled by a prescribed shape.

In the present method, the small disturbance approximation is used with the Bailey-Ballhaus finite difference column relaxation algorithm (Ref. 4). The jet exhaust plume contact jump conditions and the nacelle tangency condition are imposed in a quasi-cylindrical fashion on a prismatic surface of rectangular cross-section fitting the cartesian grid. The pylon condition is imposed in a quasi-planar manner.

The incorporation of a powered jet, with a total pressure higher than the ambient value, follows the procedure of Ehlers (Ref. 5). The jet flow is treated by a small disturbance method where the potential is defined relative to the reference velocity (V_j) attained by the isentropic expansion from the nozzle total pressure to the free stream pressure. It will be seen that in this formulation, the requirement of continuous static pressure across the jet boundary generates a jump in the potential at the interface. Column relaxations are then carried out in the usual fashion bridging the jet interface with the contact jump conditions.

The above procedure was applied to a NASA/Langley transport research model (Figure 1) with over-the-wing (OTW) nacelle/pylon and upper surface blowing (USB) nacelle configurations. In the former, two OTW configurations were calculated, an axisymmetric nacelle mounted on a symmetric pylon, and a contoured nacelle/pylon from Ref. 6 in which the outer contour was fitted to the wing/fuselage streamlines as determined by a subcritical panel method. The computed cases correspond to cases tested by NASA in the Langley 16-Foot Transonic Tunnel.

It is clear that the above subcritical streamline fitting design of the nacelle/pylon will be deficient when the configuration is immersed in

supersonic flow, particularly with a severely underexpanded jet exhaust. The measured pressure distributions for the contoured OTW configuration were analyzed to identify remaining adverse interference effects. Configuration improvements were then evolved using the computer program.

In the following sections a brief review of the small disturbance formulation of the problem and a description of the solution algorithm is presented. This is then followed by test/theory comparisons for the OTW and USB cases. Finally, the results for the redesigned OTW configuration are presented.

The authors wish to express their appreciation to Mr. W. K. Abeyounis (NASA contract monitor) and to Mr. L. E. Putnam (Assistant Chief, Propulsion Aerodynamics Branch) for their assistance during this study. Mr. E. E. Lee and Mr. O. E. Pendergraft, Jr. kindly made available the results of the wind tunnel test prior to their publication.

II. FORMULATION OF THE SMALL DISTURBANCE PROBLEM

The problem formulation follows essentially that given in Ref. 7. The perturbation potential in conservation form is given by

$$[(1-M_\infty^2)\,\phi_x - \frac{\gamma+1}{2} M_\infty^2 \phi_x^2 + (1-M_\infty^2)\,\phi_y^2]_x -$$

$$[(1-\frac{\gamma-1}{2} M_\infty^2)\,\phi_y^2]_x + [\phi_y-(\gamma-1)\,M_\infty^2\,\phi_x\phi_y]_y + [\phi_z]_z = 0 \qquad (1)$$

where ϕ is the potential defined relative to the freestream Mach number M_∞, γ is the ratio of specific heats, and x, y, and z are the cartesian coordinates, with x in the freestream direction, y in the "spanwise" direction, and z normal to the wing reference plane (Figure 1). Coordinate subscripts denote differentiation. The above equation includes higher order sweep terms to improve the swept shock jump conditions.

The flow tangency condition on the configuration surface is given by the scalar product of the surface normal and the velocity vector vanishing. In the small disturbance approximation, not only are the velocity components and the direction cosines of the surface normal simplified, but most importantly the tangency condition is imposed in a quasi-planar or quasi-cylindrical fashion on a substitute neighboring surface convenient to the mesh system. This boundary condition is given as

$$F_x + F_y\,\phi_y + F_z\,\phi_z = 0 \qquad (2)$$

where $F(x,y,z) = 0$ defines the surface of the configuration, and the partial derivatives of F are proportional to the direction cosines of the normal. In the present program, the above tangency condition is imposed on a prismatic surface of rectangular cross-section compatible with the cartesian grid, while the wing and pylon conditions are fulfilled on appropriate projection planes.

The flow within the nacelle is excluded from the calculations. Appropriate boundary conditions are therefore prescribed at the inlet and nozzle exit planes. At the inlet face, a constant value of ϕ_x corresponding to the desired inlet mass flow ratio is prescribed. At the nozzle exit plane, a constant value of $\phi_{j,x}$ is defined corresponding to the desired exit Mach number and the jet to freestream total pressure ratio, where ϕ_j is the jet perturbation potential to be defined later.

Across vortex sheets, either trailing downstream from lifting surfaces or forming the powered jet boundary, contact jump conditions must be imposed requiring both the continuity of the pressure and the streamline slopes. In the case of the trailing vortex sheets, the total pressure is the same on either side of the sheet so that the usual form of the contact jump conditions as given in Ref. 7 will prevail.

In the case of the powered jet, a modification to account for the jump in the total pressure at the jet boundary must be made. A procedure similar to the method developed by Ehlers (Ref. 5) is used. Here the jet flow is treated by a small disturbance theory with the perturbation velocity defined relative to the reference velocity V_j (with the corresponding Mach number M_j). The reference velocity V_j is obtained by an isentropic expansion from the jet total pressure to the ambient freestream pressure. The jet potential ϕ_j

then fulfills Eq. (1) with M_j and the jet specific heat ratio γ_j substituted appropriately. The second order sweep terms contained in Eq. (1) to obtain the proper shock jump conditions for the shocks occurring on swept wings are not required for the shocks expected within the jet, but these higher order terms are retained for convenience.

Consider first the requirement for the streamline slope continuity across the jet boundary. Thus if $J(x,y,z) = 0$ defines the unknown jet boundary, then the flow tangency condition at the interface is given by

$$J_x + J_y \phi_y + J_z \phi_z = J_x + J_y \phi_{J,y} + J_z \phi_{J,z} = 0 \tag{3}$$

The desired jump condition is obtained by subtracting the two equations of (3); that is,

$$J_y [\phi_y] + J_z [\phi_z] = 0 \tag{4}$$

where the square brackets denote the jump in the bracketed quantity across the jet boundary from the ambient flow to the jet flow. The unknown jet shape derivatives J_y and J_z are evaluated iteratively in terms of the cross-flow velocities using Eq. (3).

The second jump condition is obtained by the pressure continuity condition at the jet interface. The pressure within the ambient and jet flows are given in the small disturbance approximation by

$$\frac{p - p_\infty}{\frac{1}{2} \gamma p_\infty M_\infty^2} = - 2 \phi_x \tag{5}$$

$$\frac{p_j - p_\infty}{\frac{1}{2} \gamma_j p_\infty M^2_j} = - 2 \phi_{j,x}$$

Equating the pressures at the interface ($p = p_j$), we obtain

$$\gamma M_\infty^2 \phi_x = \gamma_j M_j^2 \phi_{J,x} \tag{6}$$

or integrating with respect to x, we obtain

$$\gamma M_\infty^2 \phi - \gamma_j M_j^2 \phi_j = C(y,z), \tag{7}$$

where $C(y,z)$ is the constant of integration which is evaluated using the pressure continuity at the nozzle exit in terms of the prescribed nozzle exit value of $\phi_{j,x}$.

The jet exhaust contact jump conditions (4) and (7) are prescribed quasi-cylindrically on the downstream extension of the surface of rectangular cross-section used for the nacelle.

The far downstream condition requires a uniformity of the pressure and is given by

$$\phi_x = \phi_{J,x} = 0 \tag{8}$$

At the remainder of the far-field boundaries the asymptotic far-field solution is prescribed.

III. DIFFERENCE ALGORITHM

The numerical procedure used is the successive line over-relaxation (SLOR) method developed by Bailey and Ballhaus. Since this procedure is described in detail in Mason, etc., (Ref. 7), in the present section only brief comments on those aspects not covered in the above reference are given.

It may be recalled that the nacelle and powered jet conditions are imposed on a surface of rectangular cross-section relative to which the cartesian grid is constructed. This boundary, consistent with the other internal boundaries, is placed midway between the grid lines.

The tangency condition at the nacelle surface is given by Eq. (2). Along the "horizontal sides" of the nacelle, the boundary condition is

$$\phi_z = - F_z^{-1} (F_x + F_y \phi_y) \tag{9}$$

where ϕ_y is evaluated from a prior iteration. The role of the velocity components is switched for the "vertical surfaces" of the nacelle. The numerical implementation of these conditions would then be identical to that for the wing or fuselage described in Ref. 7.

The contact jump conditions at the powered jet boundary are given by Eqs. (4) and (7) and are numerically implemented as in the case of the trailing vortex sheet downstream of the wing with the following minor modifications. First in the jump condition (4) for the continuity of streamline slopes, an explicit condition for the jump of either velocity component is obtained

as in the case of the nacelle condition described above. The a priori unknown direction cosines J_y and J_z are determined iteratively using a circular cross-section as an initial guess. Updated values of the direction cosines are then obtained from Eq. 3 using the resulting cross-flow velocities. In the case of the pressure continuity, the jump in the potential given by Eq. (7) replaces the constant jump prevailing along a trailing vortex.

IV. APPLICATIONS

Examples illustrating the use of the above procedure are next given for a NASA Transport Research Model (Figure 1) for the OTW nacelle/pylon and the USB nacelle configurations. The wing sweep for this model is 30° at the quarter chord, the aspect ratio 8, the taper ratio 0.30, and the airfoil section a NASA supercritical section. The airfoil thickness varies from 16 percent at the root to 12 percent at the tip, with a linear washout of 4.5°. The nacelle and pylon are located nominally at 0.25 semi-span.

Wind tunnel tests on this model were carried out by NASA/Langley in the 16-Foot Transonic Tunnel with E. Lee as the principal investigator. Balance measurements and extensive pressure measurements on the wing, nacelle, and pylon were taken. The Reynolds number based on the mean chord of 20.68 cm (8.14 in) was 2.30×10^6 for the freestream Mach number $M_\infty = 0.80$. In order to match the boundary layer thickness to wing chord ratio at the wing trailing edge for flight Reynolds numbers, the transition was fixed as a function of spanwise location. (On the upper surface, transition varied from 0.15c at $\eta = 0.154$, to 0.40 c at the break, to 0.35 c at the tip. Transition on the lower surface was at a constant 0.40 c).

The calculations were carried out at $M_\infty = 0.80$ and the design $C_L = 0.45$. Because of the known deficiencies of small disturbance methods in handling the large slopes near the wing leading edge and viscous effects in the trailing edge region, the calculations were first carried out for the wing/fuselage, changing the wing shape in the leading and trailing edge regions as well as the angle of attack to match the measured pressure distributions. The nacelle and pylon were then added to this tailored wing. The shape changes are

intended to compensate for the small disturbance approximation, and in the aft region, also for the viscous displacement effects. The viscous interactions at the shock were incorporated by inserting at each iteration an appropriate wedge-nosed ramp at the base of the supersonic-subsonic shocks to simulate the boundary layer displacement.

In Figure 2, a comparison is made of the pressure distributions for the wing/fuselage, with and without the shape and angle of attack modifications, with the measured distributions at several spanwise stations (η). The experimental angle of attack was $\sim 0.60^{\circ}$ while the modified value was 2.0°. The shape modifications at several span stations are shown in Figure 3. Since a design computer program was not available, the shape changes were evolved by trial and error using the analysis code. The results of Figure 2 show that the measured pressures were reasonably recovered by the shape changes particularly in the region to be occupied by the nacelle/pylon. Remaining test/theory mismatches include the aft lower surface pressures and the weak shock on the upper surface in the midchord region. The viscous ramp and shape changes were used to incorporate the viscous effects in these regions.

The OTW symmetric nacelle/pylon was next added to the tailored wing, and the resulting pressure distributions with and without the viscous ramp are shown in Figure 4. The planar viscous ramp procedure of Ref. 8 was incorporated normal to the shock. The sweep of the shock was approximated from pressure distributions of earlier iterations. The test/theory comparison is satisfactory on the upper surface though it does not agree as well on the lower surface. It is seen here that the presence of the nacelle/pylon generated a strong, essentially unswept shock inboard of the pylon with an upstream Mach number surpassing 1.40. Undoubtedly a severe shock-induced

separation occurs. The cause for this shock will be discussed in a later section.

The pressure distributions for the case of the OTW contoured nacelle/pylon (shaped to fit the subcritical streamlines for the wing/fuselage) are shown in Figure 5 and compared to the results with the pylon removed. The test/theory comparison shows an excellent match on the wing upper surface inboard of the pylon with less satisfactory agreement outboard. Figure 6 compares the symmetric and contoured nacelle/pylon shapes. Contouring significantly weakens the upper surface shock inboard of the pylon, reducing the pre-shock Mach number M_1 from 1.40 to 1.30 at 0.154 semi-span. However, the secondary effect of the pylon is the moderate strengthening of the upper surface shock outboard of the pylon.

In the above calculations the jet exhaust reference Mach number M_j was set equal to the freestream Mach number M ; that is, $M_j = M_\infty = 0.80$. This then represents an unpowered case. Additionally, a choked convergent nozzle was assumed. In this case the nozzle exit flow was underexpanded since the sonic exit flow exhausted into the ambient supersonic region of the wing. The resulting "compression corner" formed by the outward spreading jet boundary at the nozzle exit then served to anchor the wing shock wave.

In the case of the powered jet (M_j greater than M_∞), an increase of the jet plume spreading at the nozzle exit relative to the unpowered case will occur, leading to a stronger oblique shock at the nozzle/plume corner. (The increased entrainment of the powered jet would tend to lessen the shock; however, plume blockage effects would be predominant.) To illustrate the effect of the powered jet, the OTW symmetric nacelle/pylon configuration for

M_J = 1.20 was next calculated, and the results are shown in Figure 7. The sonic nozzle was retained, and the ratio of specific heats for the jet exhaust flow was kept at 1.4. The corresponding jet plume shapes in a vertical cut as well as the plume "center line" pressure variation are shown in Figure 8.

A test/theory comparison for the uncontoured USB nacelle configuration is shown in Figure 9. General features of the observed interference effects have been obtained in the calculations, but there are significant quantitative differences. The latter in large part is due to the difficulty of defining the nacelle slopes in the simplified formulation of the boundary condition. Omission of the fairing below the nacelle (see Figure 1) in the calculations also has contributed to the test/theory mismatch.

By comparing these results with those of the uncontoured OTW case of Figure 4, it is seen that eliminating the space beneath the nacelle and removing the pylon significantly reduces the adverse interference of the engine installation on the wing upper surface inboard of the pylon. On the other hand, an added scrubbing drag of the jet on the wing must be expected for the USB case. Since the jet exhausts into the wing supersonic region in the above USB configuration, an interference shock is generated by the underexpanded plume. Such an interference shock can be minimized or avoided by moving the nozzle exit further downstream to where the flow is subcritical.

V. ANALYSIS OF THE OTW CONFIGURATIONS

In the present section, wind tunnel data for the OTW configurations at $M_\infty = 0.80$ and $C_L = 0.45$ are analyzed to determine the nature of the nacelle/pylon interference and to evolve additional configuration improvements.

The lift curve and the drag polar for the wing/fuselage and for the symmetric and contoured nacelle/pylon configurations are shown in Figure 10. It is seen here that the addition of the nacelle/pylon has decreased the lift such that in the linear range approximately one-third degree greater angle of attack is required to achieve the wing/fuselage lift. The addition of the symmetric nacelle/pylon has increased the drag by approximately 140 counts at the lift coefficient of 0.45. (Here one count of drag is equal to $C_D = 0.0001$.) The subcritical streamline contouring of the nacelle/pylon reduced this interference drag by approximately 50 counts to 90 counts of added drag remaining.

The cause for this drag increase may be seen by comparing the wing pressure distributions at span stations in the vicinity of the pylon given in Figures 2, 4 and 5. It is seen that the addition of the nacelle/pylon has generated a significant second supersonic expansion on the inboard side of the pylon which is terminated by a strong shock. A moderate shock was generated on the outboard side of the pylon. The nature of these shocks can be seen more directly from the pylon pressures shown in Figure 11. The inboard pylon pressures indicate the presence of a severe shock-induced separation resulting in a lambda shock. The contouring of the nacelle/pylon has significantly weakened the inboard shock, but strengthened the outboard shock. The resulting shock wave and separated region are sketched in Figure 12.

A plausible explanation of the effect of the nacelle/pylon on the pressure distribution described above can be explained as follows. First, consider only the effect of adding the nacelle, and treat the flow as planar. The actual flow will be moderated from this planar picture by the lateral three dimensional effects. In the lower part of Figure 13, the flow structure for the case of the wing alone is shown. A concentrated family of expansion waves is generated in the nose region. These expansion waves travel to the sonic line where they are reflected as compression waves. The resulting compression waves reimpinge on the airfoil where they are reflected as compression waves. The strength of the latter compression waves will depend upon the surface curvature at the point of impingement, with the reflected compression wave being stronger with decreased surface convexity. Thus for each nose expansion wave as WX of Figure 13, a double compression wave will result at a further downstream point Y. The flow passing through these double compression waves will decelerate leading to the moderate pressures arising in the case of the wing/fuselage.

When the nacelle surface is present, many of the nose expansion waves (as BC) will be reflected at the nacelle lower surface as expansion waves. Again, the strength of the reflected waves will depend upon the nacelle surface curvature at the impingement point. These reflected expansion waves now reimpinge on the airfoil surface, reflecting there as expansion waves. The cumulative effect of these double expansion waves are in large part responsible for the second supersonic expansion seen earlier in the midchord region of the wing.

In Figure 13, both the symmetric (dashed line) and the contoured (solid line) nacelles are shown. Along the nacelle surface AE, the curvature was changed from a convex to a concave curvature as a result of the nacelle contouring. This change of the curvature will produce compression perturbation waves which will impinge on the airfoil surface to produce the observed lessening of the second supersonic expansion.

Consider next the effect of adding the pylon to the above wing/nacelle configuration. In Figure 13 we show the contoured and the symmetric pylon cross-sections. The contoured shape represents the wing-alone streamlines. It is seen that on the inboard side of the pylon, the wing-alone streamlines are concave. If now these streamlines are constrained to follow the straight symmetric pylon surface, the result is a reduction of the streamline concavity and the generation of perturbation expansion waves. The opposite effect should be expected on the outboard side. Thus the result of adding the symmetric pylon is to worsen the interference on the inboard side and reduce it on the outboard side.

The fact that the contoured nacelle/pylon did not eliminate the adverse interference is due to the inadequacy of the subcritical panel method to predict the supercritical streamlines, as well as to the impossibility of fitting adequately the nacelle and pylon of finite thickness together with their viscous displacement effects to the wing-alone streamlines. In the flow-through nacelle case considered earlier, the jet exhaust is underexpanded; that is, the pressure at the nozzle exit is higher than the surrounding ambient flow. The jet spreads laterally distorting the streamlines away from the wing-alone streamlines, thereby creating an interference.

The measured pressures for the symmetric and contoured nacelle/pylon configurations when compared to the wing/fuselage pressures clearly point to the cause of the unfavorable interference; namely the appearance of a greatly strengthened shock and the accompanying extensive separation of the boundary layer on the wing upper surface inboard of the pylon. The source of the enhanced supersonic expansion is the concentrated family of expansion waves generated in the leading edge region of the wing. As a first step, this expansion can be moderated by reducing the leading edge radius and incorporating a nose-down camber at the wing leading edge. Secondly, such cambering must be incorporated with minimal increase of convexity in the region under the nacelle, delaying the unavoidable addition of convexity to points on the wing downstream of the nozzle exit plane where the flow is subcritical. This nose-down camber further provides an upwind-facing surface on which the upper surface suctions can act to provide thrust.

Calculations were carried out with such a modification to the leading edge section inboard of the pylon using the NACA 64A416 airfoil as shown in Figure 14. A chord extension also has been incorporated to reduce the thickness ratio of the airfoil section. In Figure 15, the resulting pressure distributions are compared to the contoured case from Figure 5. The results indicate a significant reduction of the shock strength inboard of the pylon.

VI. CONCLUDING REMARKS

In summary, a transonic small disturbance computer program to handle wing/fuselage configurations with a nacelle, pylon, and powered jet exhaust was developed, and its use demonstrated by examples. A key simplification was the prescription of the nacelle and powered jet conditions quasi-cylindrically on a surface conformal to the cartesian grid.

The examples treated were extreme for the small disturbance theory. As compensation, wing shape changes in the leading and trailing edge regions were made such that the measured pressures for the wing/fuselage were matched. The resulting aft shape changes would compensate as well for the aft boundary layer displacement and wake effects. The shock-boundary layer interactions were incorporated by the viscous ramp method. This procedure yielded satisfactory results but was restricted to supersonic to subsonic shocks. The wing shape changes and the angle of attack correction were determined by trial and error using the analysis code. It would be desirable to have a suitable design code for this purpose.

The nacelle/pylon configurations were mounted on the tailored wing. Such a procedure permits the extended use of the small disturbance method to difficult problems frequently arising in practice. The test/theory comparisons in general were satisfactory, though there were mismatches outboard of the nacelle/pylon which were not insignificant.

It is clear that the quasi-planar or quasi-cylindrical fulfillment of the wing, nacelle, or pylon boundary conditions leads to shortcomings of concern. Thus in the NASA transport model considered, replacing the thick pylon by a

zero thickness plate creates additional flow domains within which significant distorting interference flows take place. There is further the problem of fitting the rectangular computational nacelle to the actual nacelle, this being particularly acute for the contoured nacelle. Finally important local flows were lost using the simplified boundary conditions as, for example, at the intersection of the pylon with the wing leading edge.

Despite these shortcomings, promising results were nevertheless obtained which can serve usefully in the pre-design stage of the vehicle design. Clearly more exact theories are also needed as the full potential method capable of treating configurations with high by-pass engine installations with a powered jet exhaust and with important viscous interactions.

REFERENCES

1. Boppe, C. W. and Stern, M. A. "Simulated Transonic Flows for Aircraft with Nacelles, Pylons, and Winglets," AIAA Paper 80-0130, January 1980.

2. Yu, N. J., "Transonic Flow Simulations for Complex Configurations with Surface-Fitted Grids," AIAA Paper 81-1258, 1981.

3. Jameson, A. and Caughey, D. A., "A Finite Volume Method for Transonic Potential Flow Calculations," Proc. of AIAA 3rd Computational Fluid Dynamics Conference, pp. 35-54, 1977.

4. Ballhaus, W. F., Bailey, F. R. and Frick, J., "Improved Computational Treatment of Transonic Flow About Swept Wings," Advances in Engineering Sciences, NASA CP-2001, 1976.

5. Ehlers, E. "A Numerical Method for Computing the Transonic Fan Duct Flow Over a Centerbody into an Exterior Free Stream," Boeing Document D6-41078, 1973.

6. Gillette, W. B., Mohn, L. W., Ridley, H. G., and Nark, T. C. "Upper Surface Blowing Nacelle Design Study for a Swept Airplane at Cruise Condition," NASA CR-2427, September 1974.

7. Mason, W. H., et al, "An Automated Procedure For Computing the Three-Dimensional Transonic Flow Over Wing-Body Combinations, Including Viscous Effects," AFFDL-TR77-122, 1977.

8. Jou, Wen-Huei and Murman, E. M., "A Phenomenological Model for Displacement Thickness Effects of Transonic Shockwave Boundary Layer Interactions," AGARD Symposium on Computation of Viscous-Inviscid Interactions, 1980.

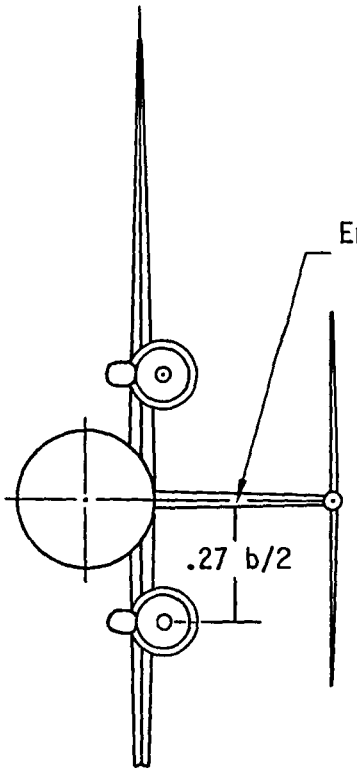

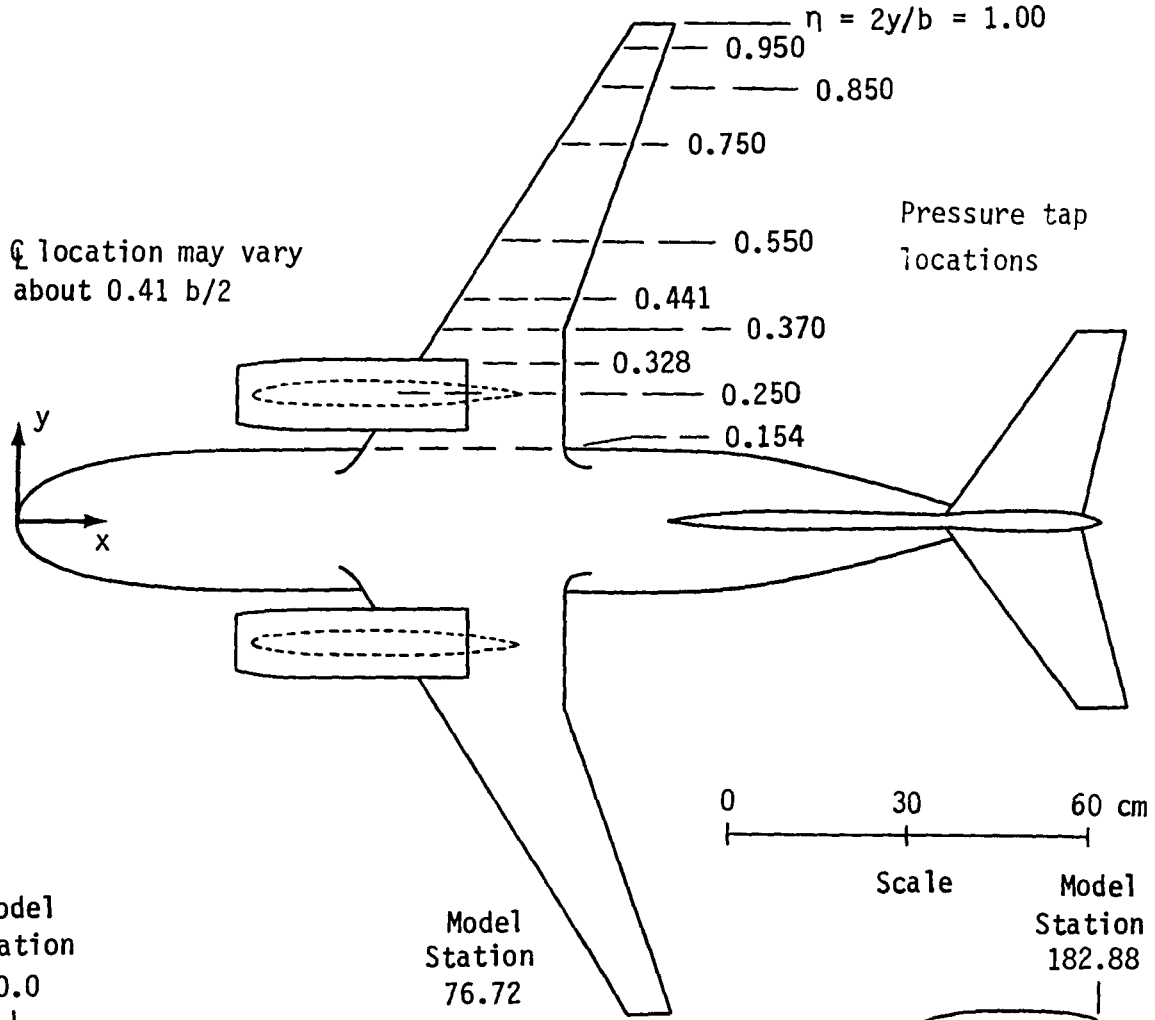

Model Geometry

Fuselage length	157.5 cm
Length overall	183.4 cm
Taper ratio	0.30
Span	150.9 cm
Aspect ratio	8.0
Sweep at 0.25c	30^{o}
Area (ref.)	2844.6 cm^2
Area (tot.)	3204.1 cm^2
Root chord (ref.)	29.0 cm
Root chord with ext.	40.6 cm
MAC	20.7 cm
t/c-root to MAC	0.16
t/c-tip	0.12
Tip chord	8.7 cm

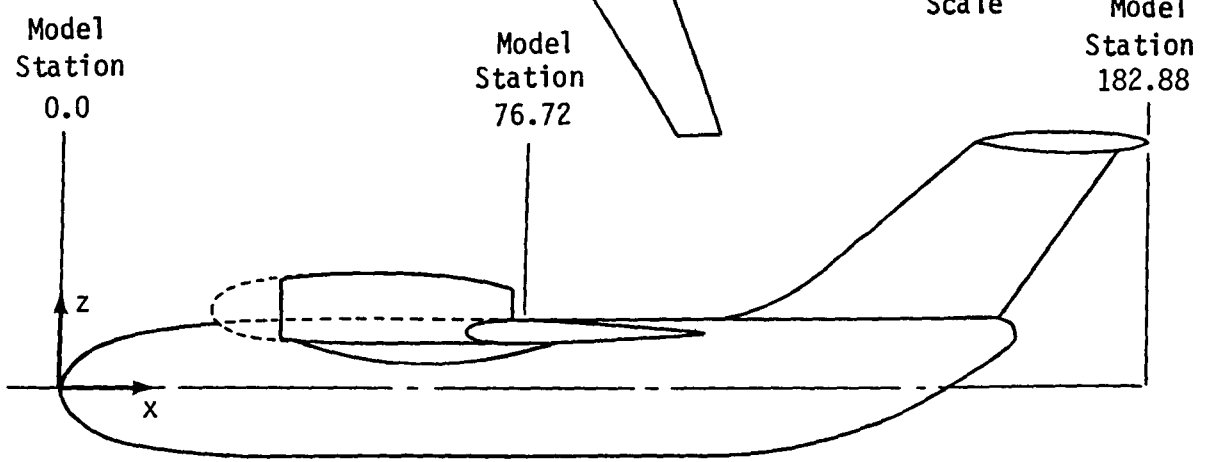

a) Upper Surface Blowing Nacelle

Figure 1 NASA/Langley Research Transport Model

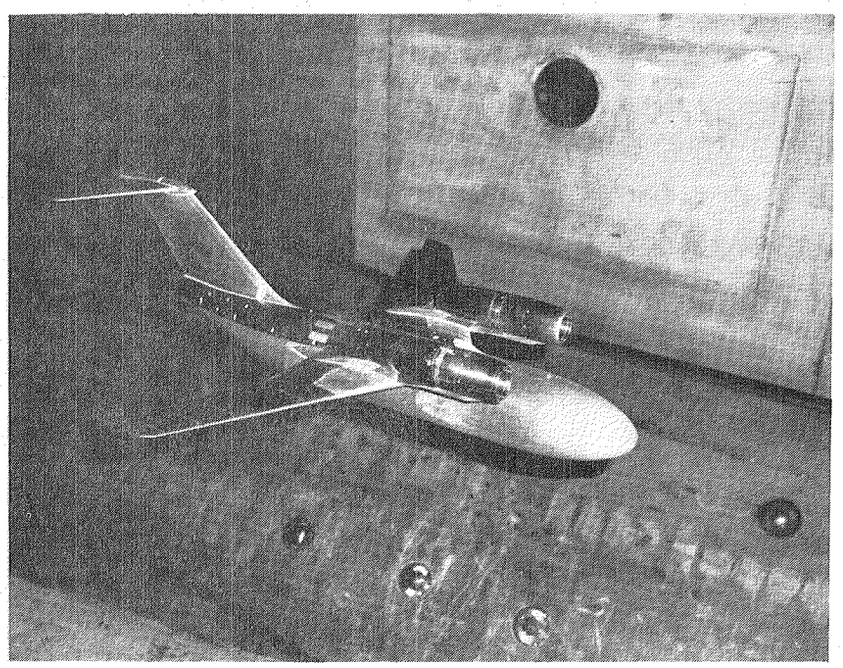

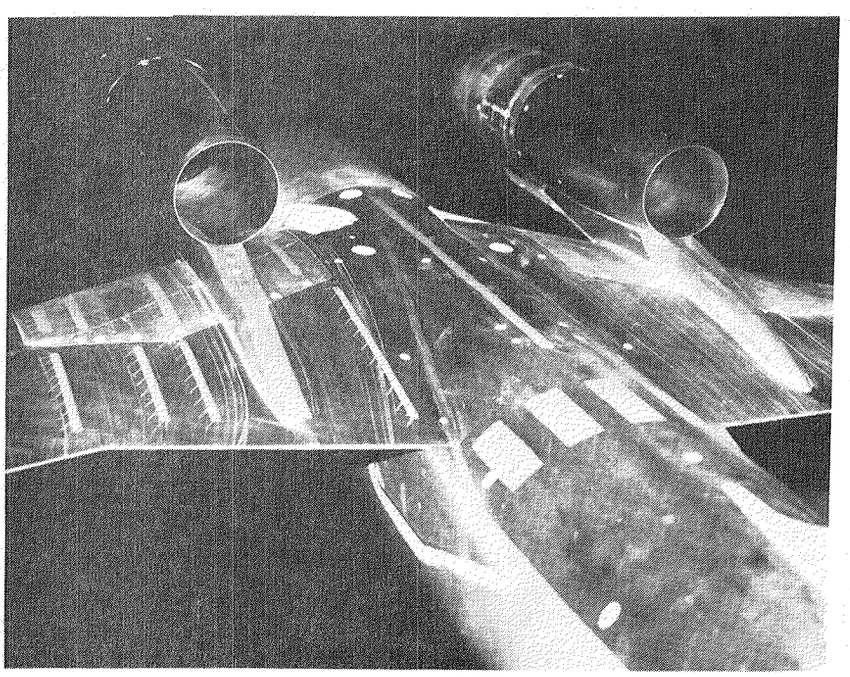

(b) Over-the-Wing Nacelle and Pylon

Figure 1 Concluded

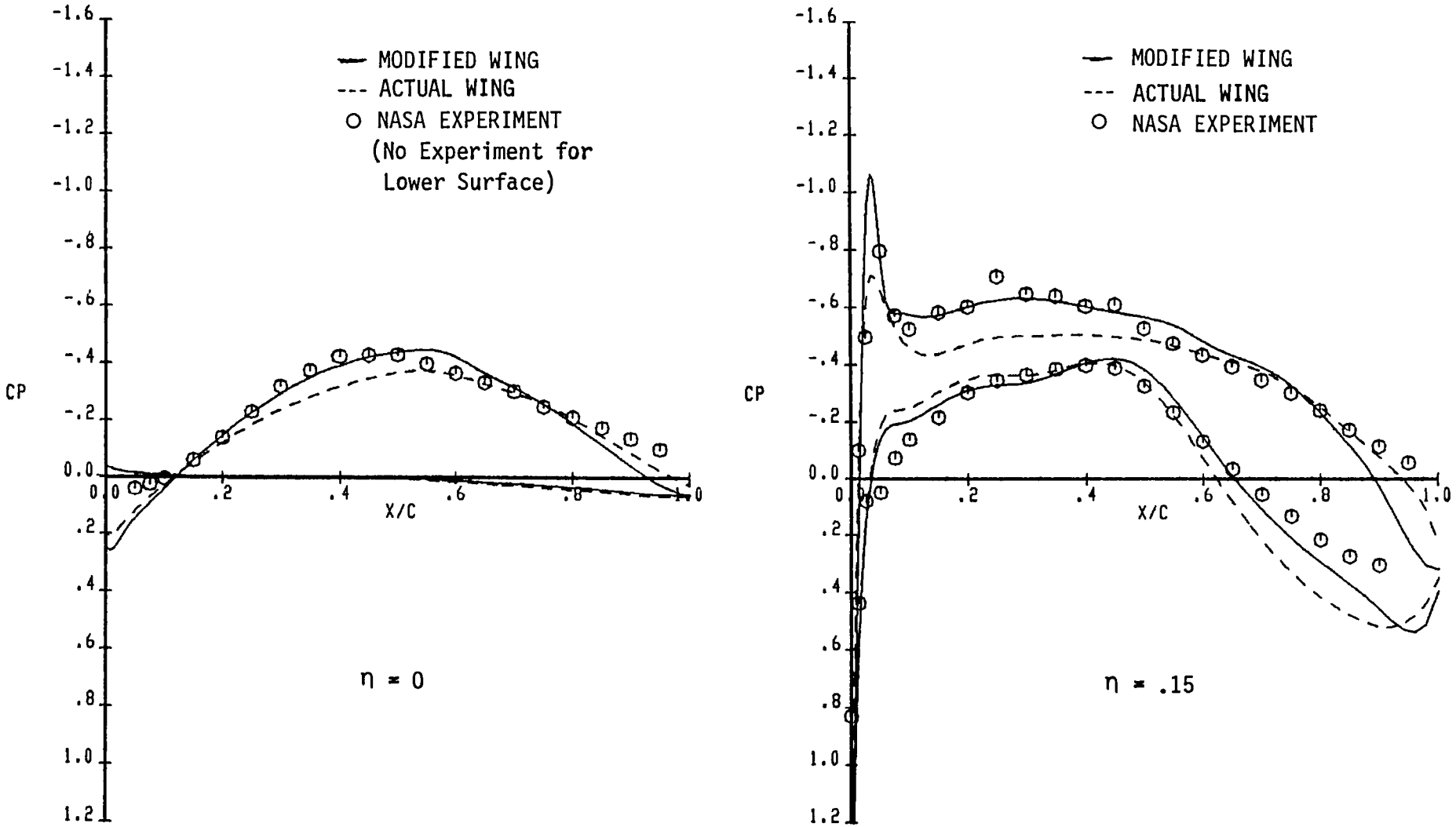

Figure 2 Pressure Distribution of Wing/Fuselage Configuration
($M_\infty = 0.80$, $C_L = 0.45$)

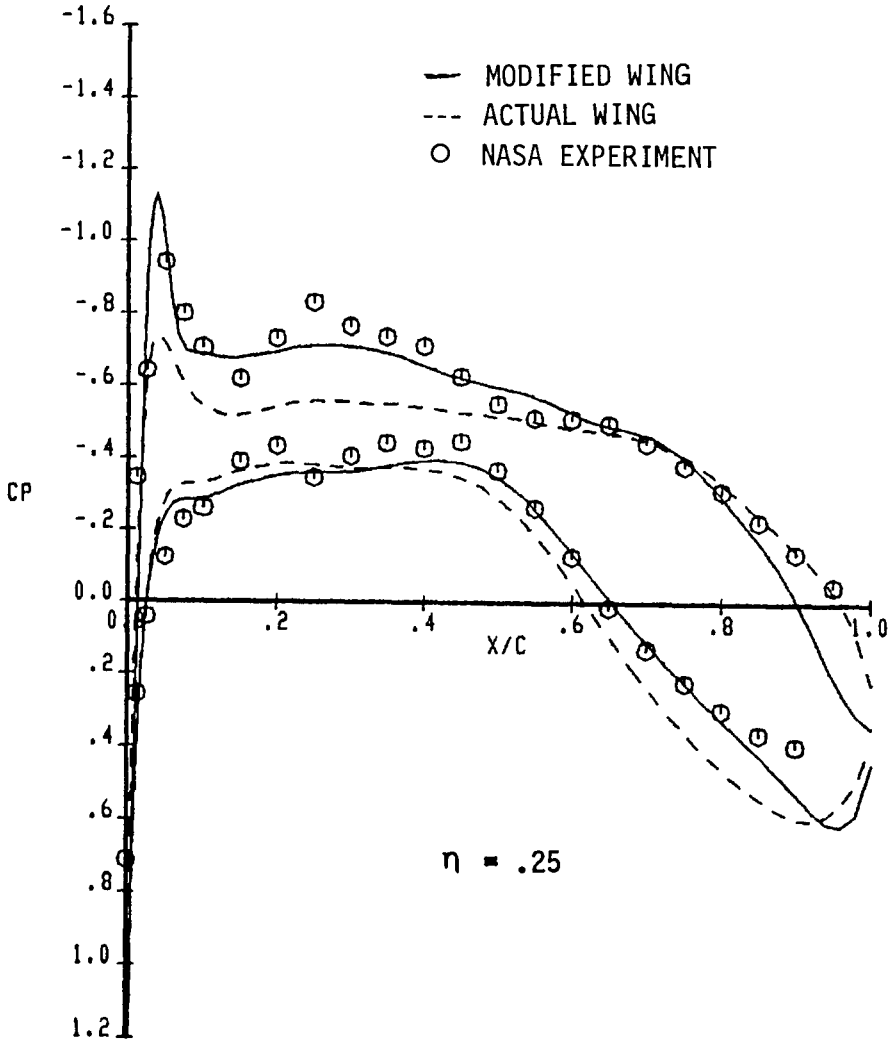

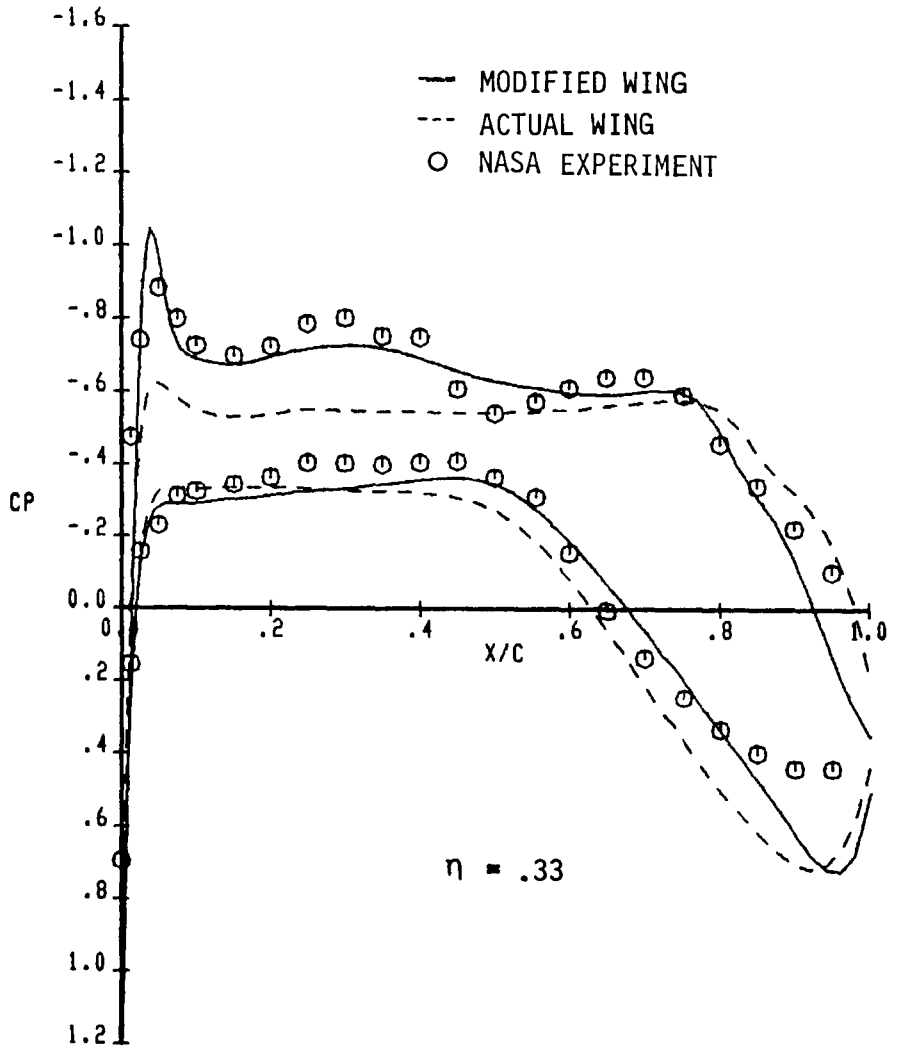

Figure 2 Continued

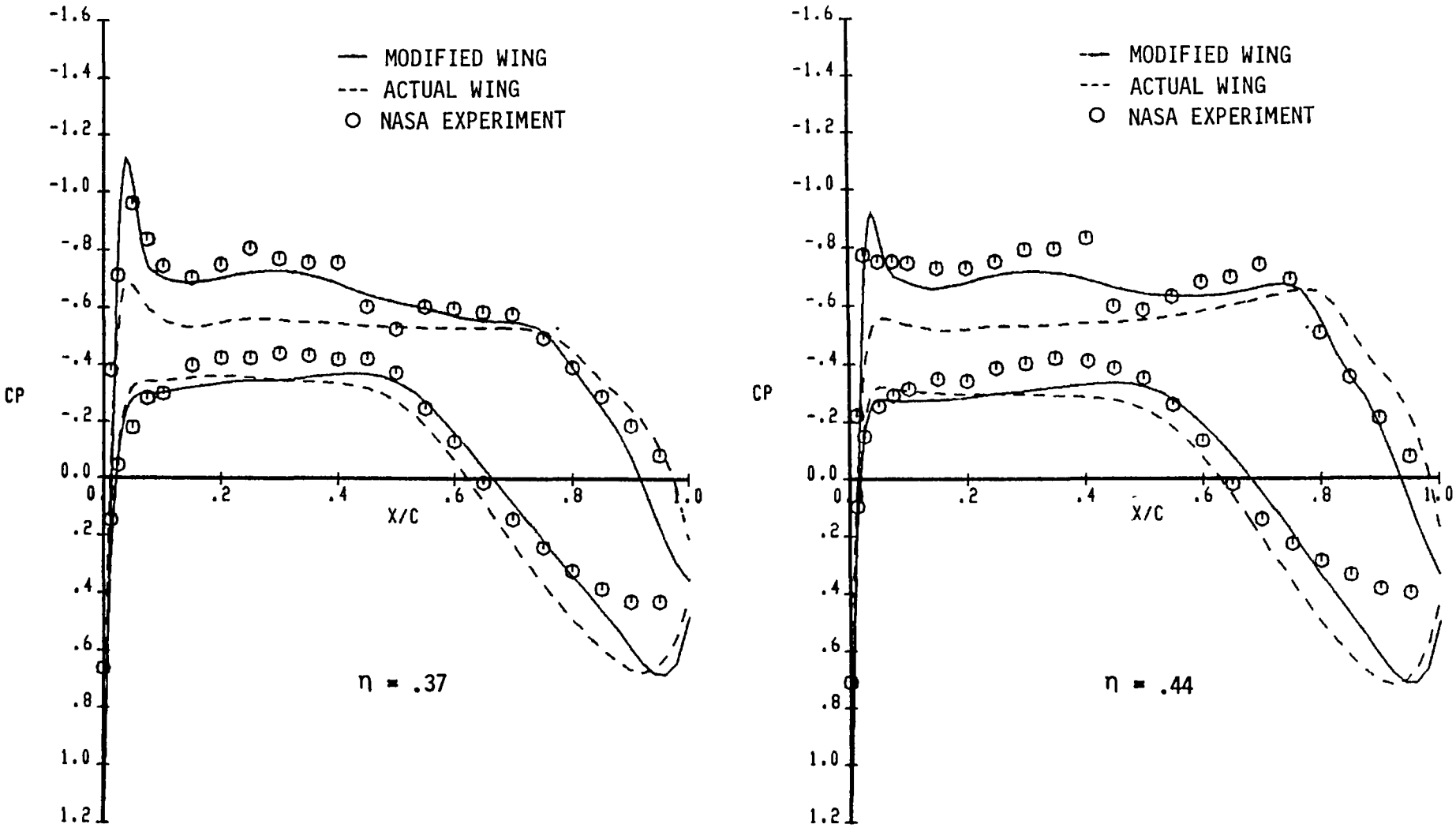

Figure 2 Continued

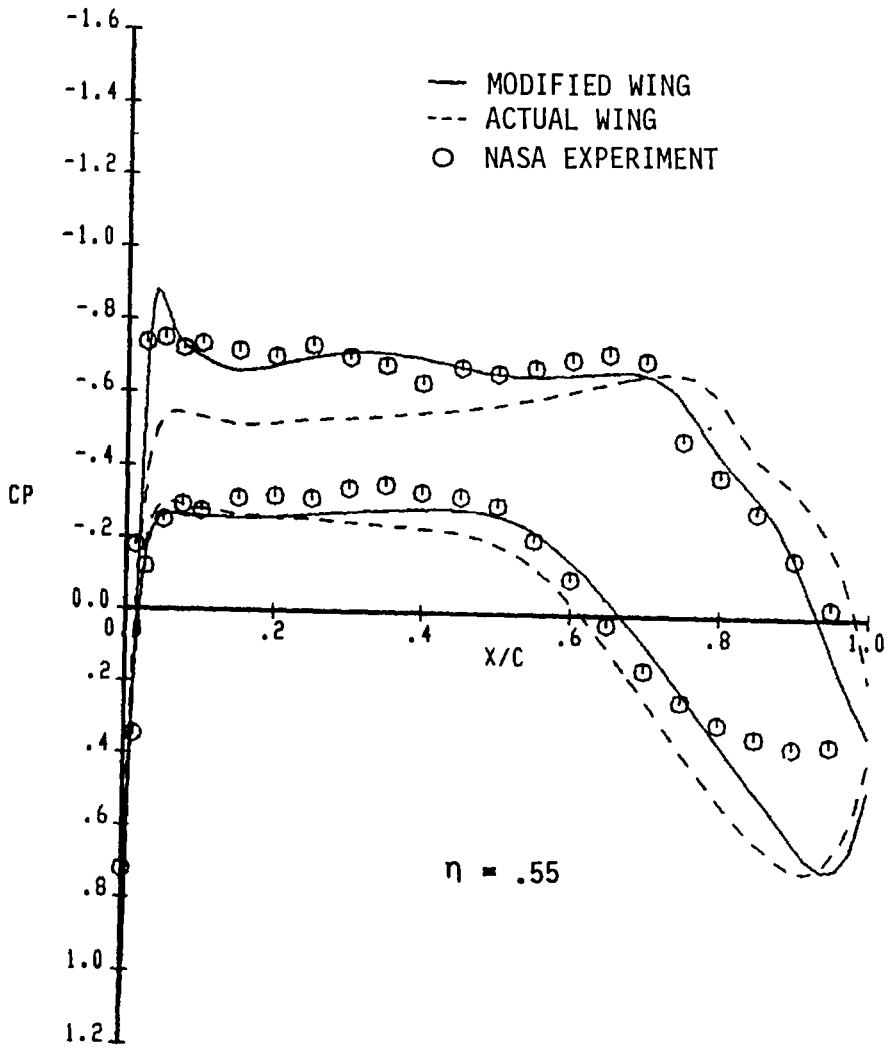

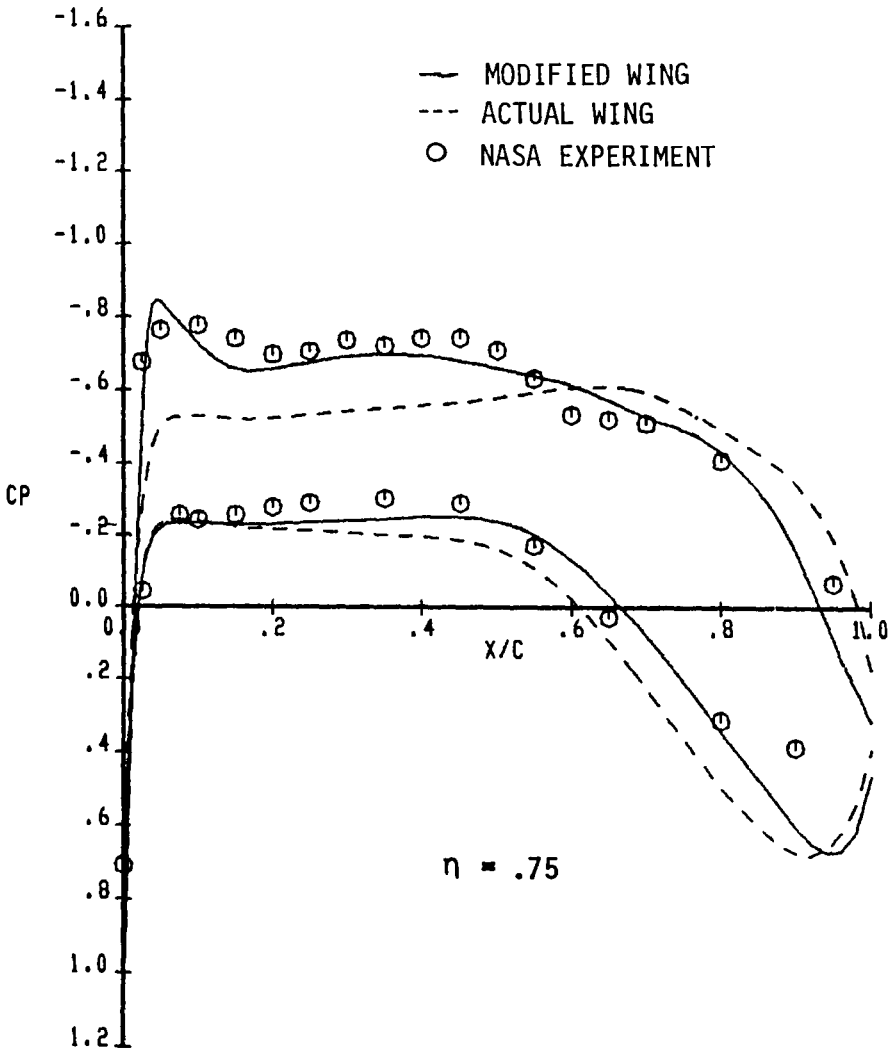

Figure 2 Continued

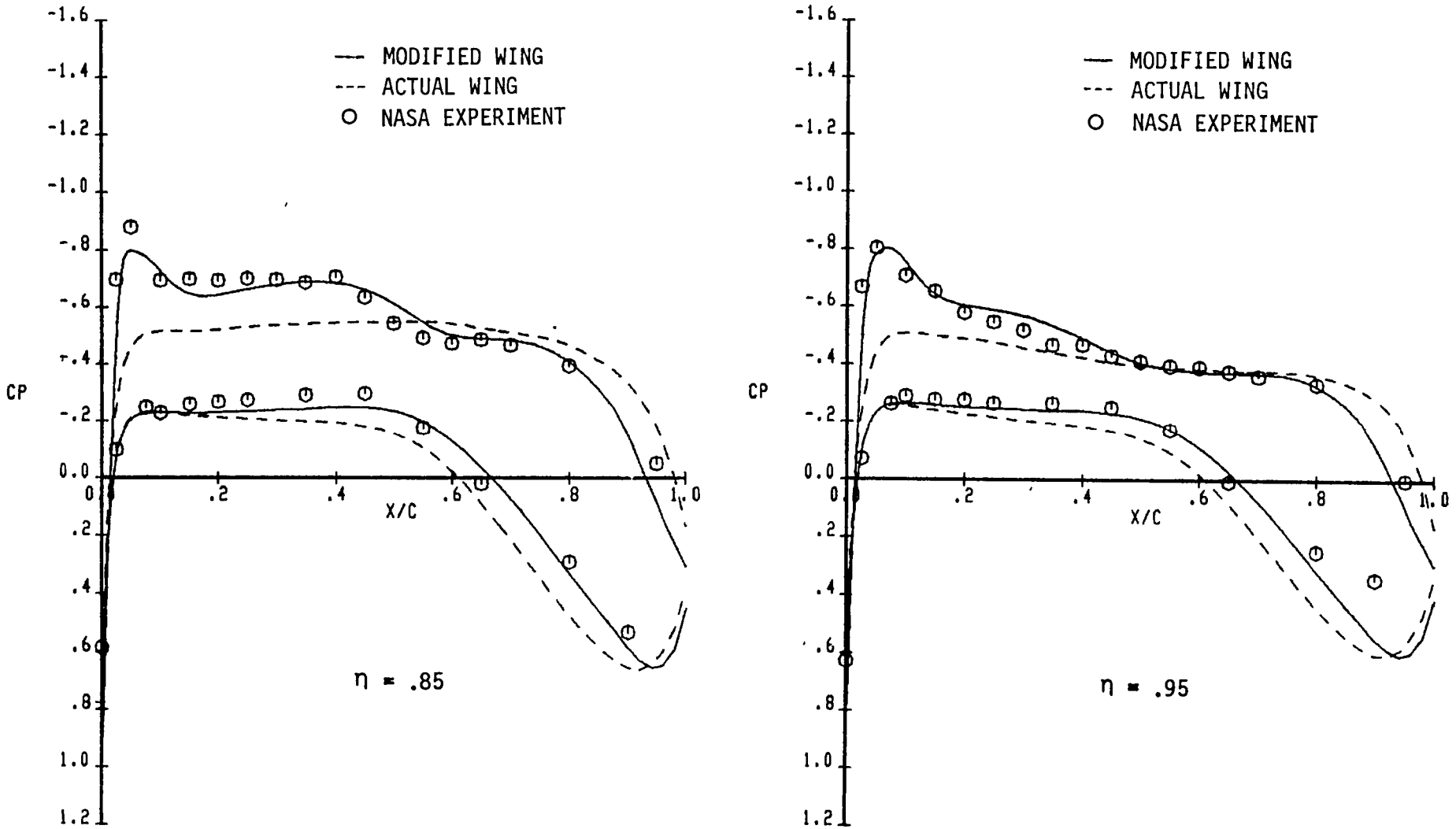

Figure 2 Concluded

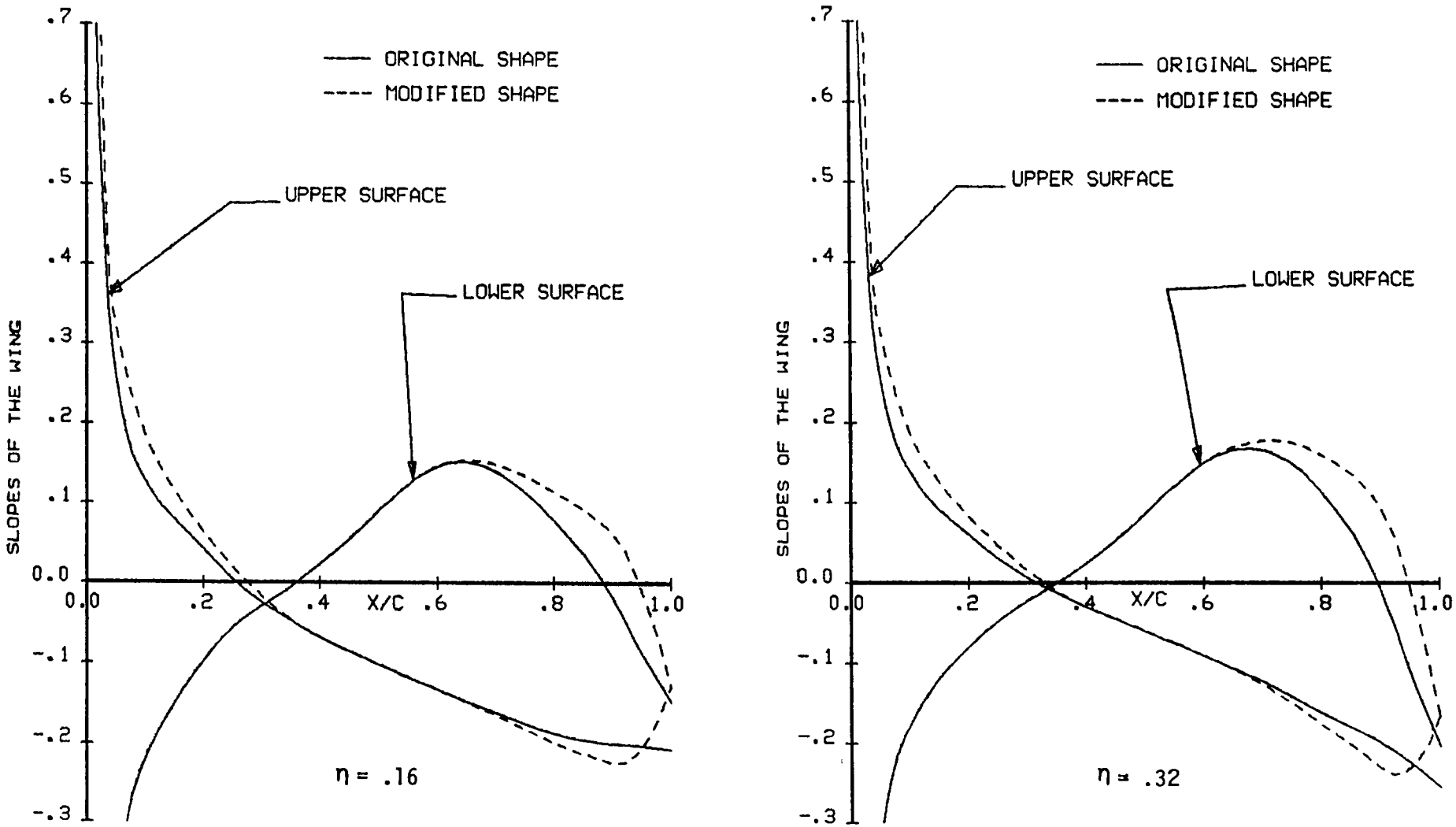

Figure 3 Comparison of the Slopes of the Wing between the Original and Modified Shapes

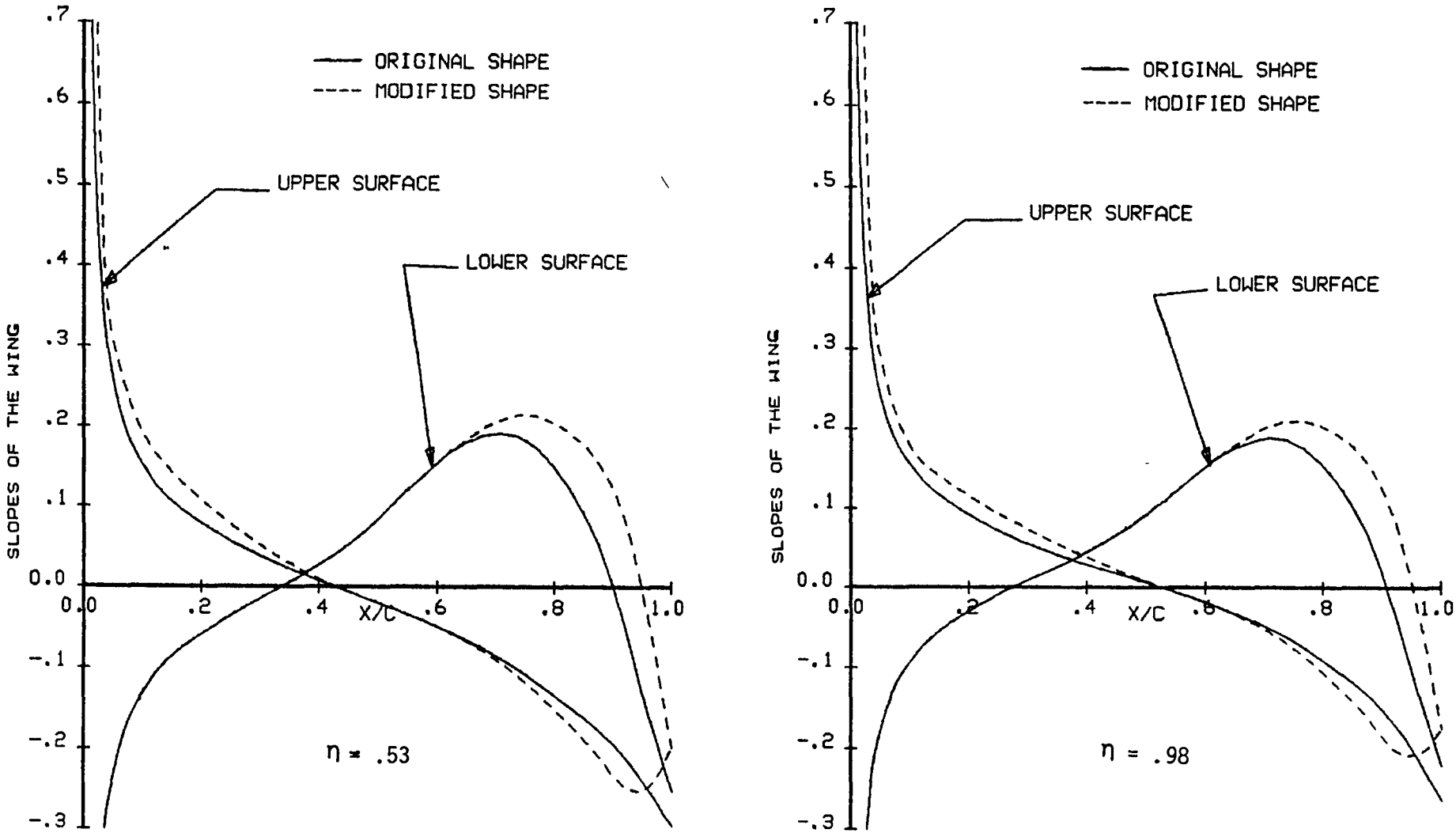

Figure 3 Concluded

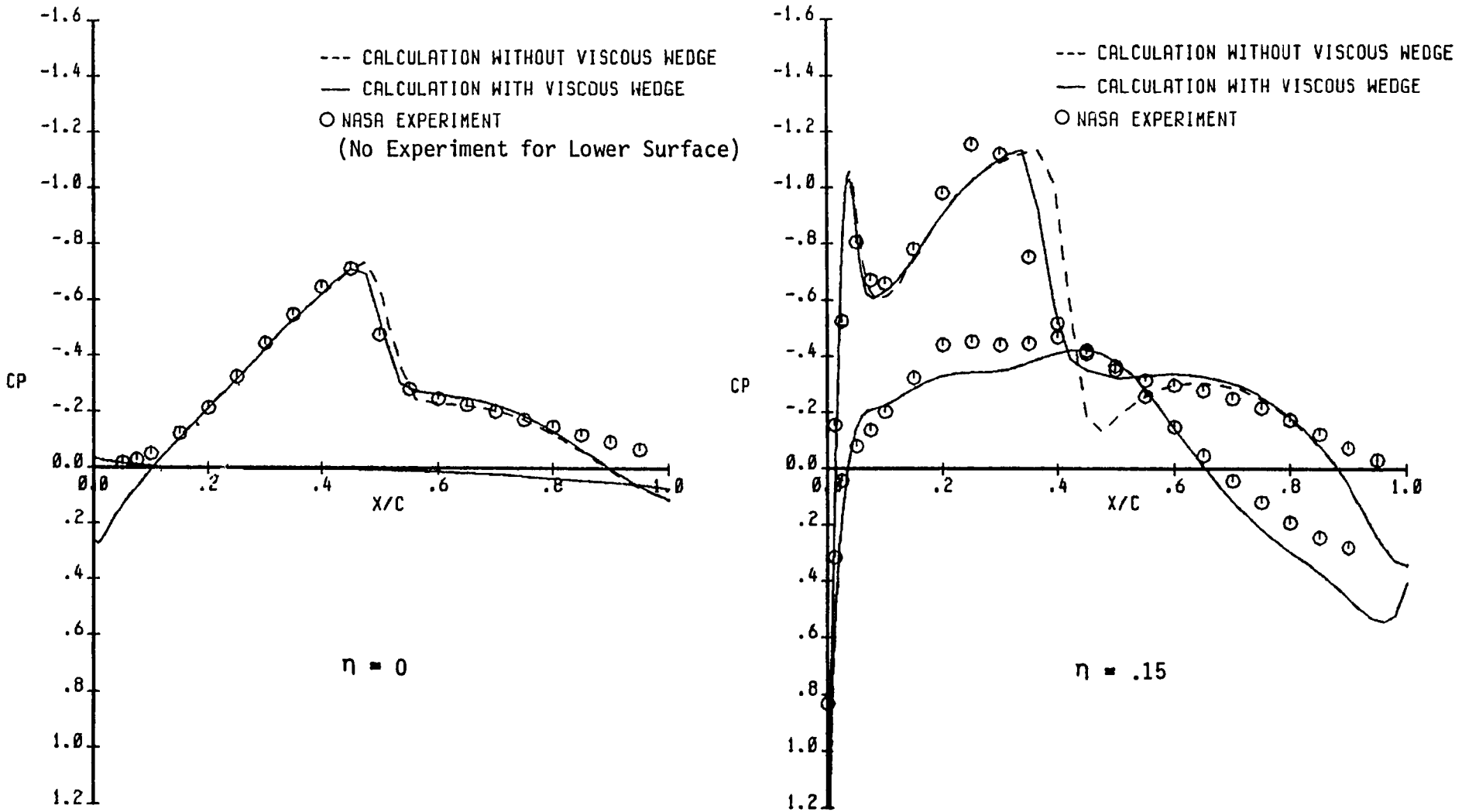

Figure 4 Pressure Distribution of OTW Symmetric Nacelle/Pylon Configuration
(M_∞ = 0.80, C_L = 0.45)

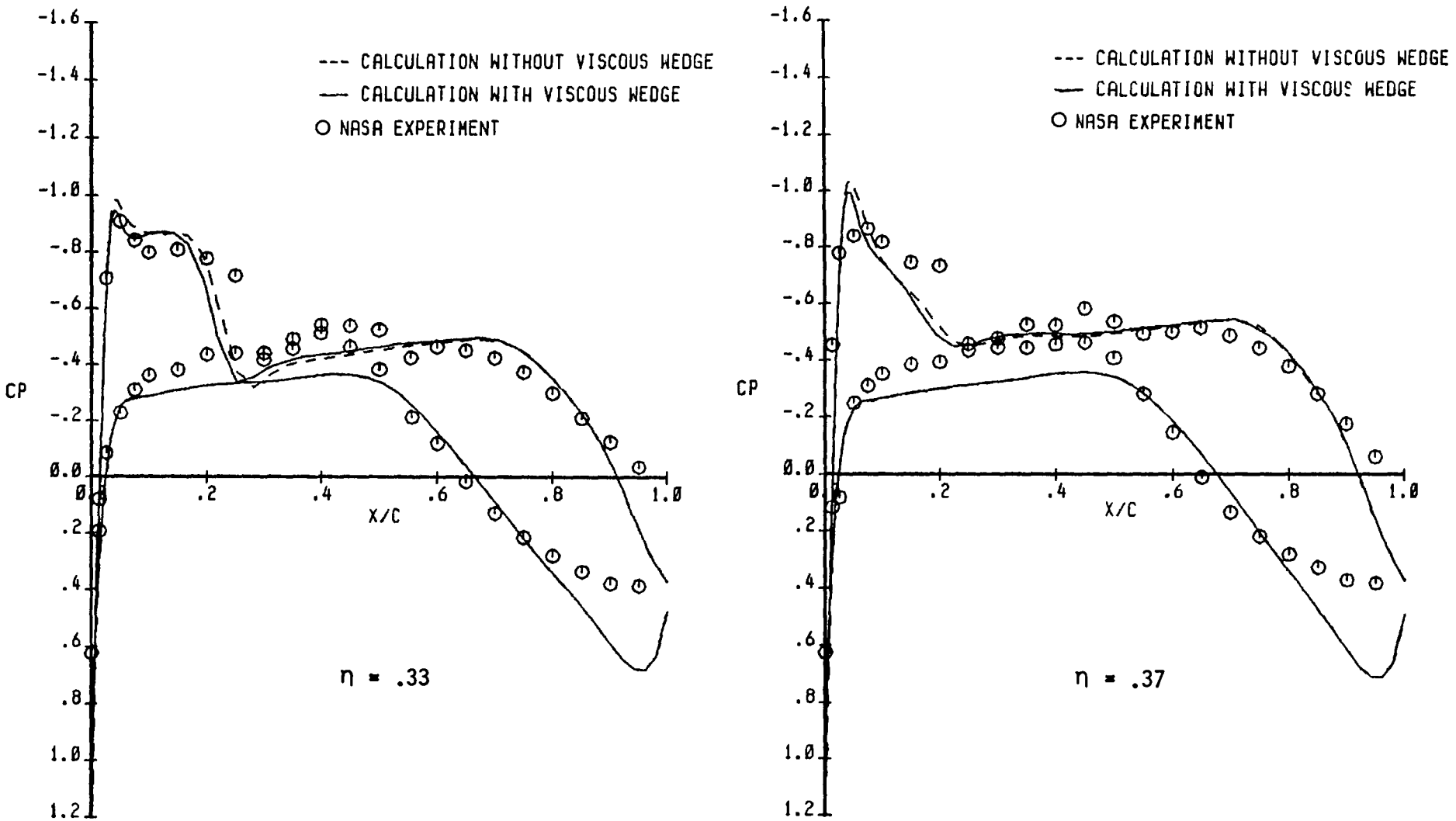

Figure 4 Continued

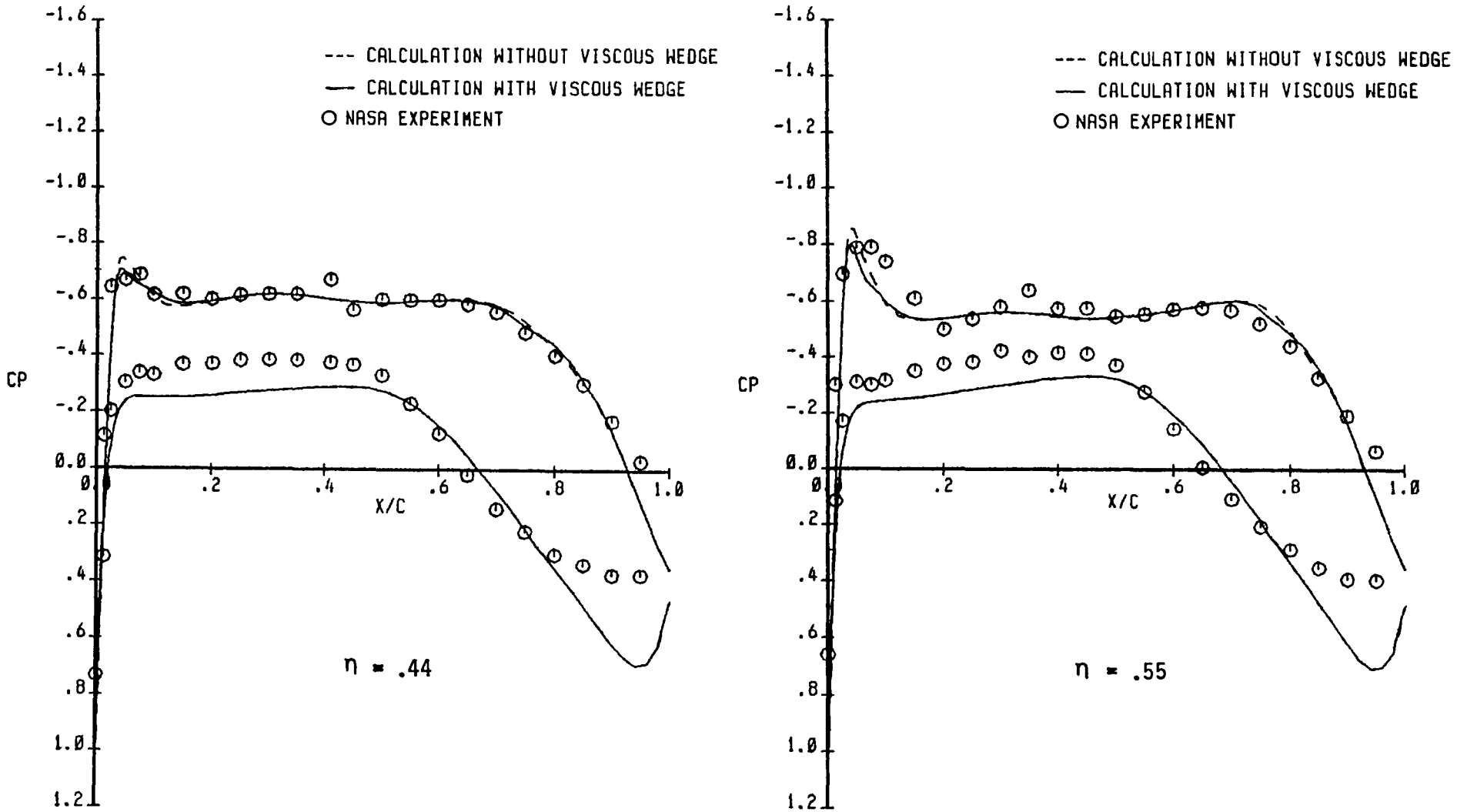

Figure 4 Continued

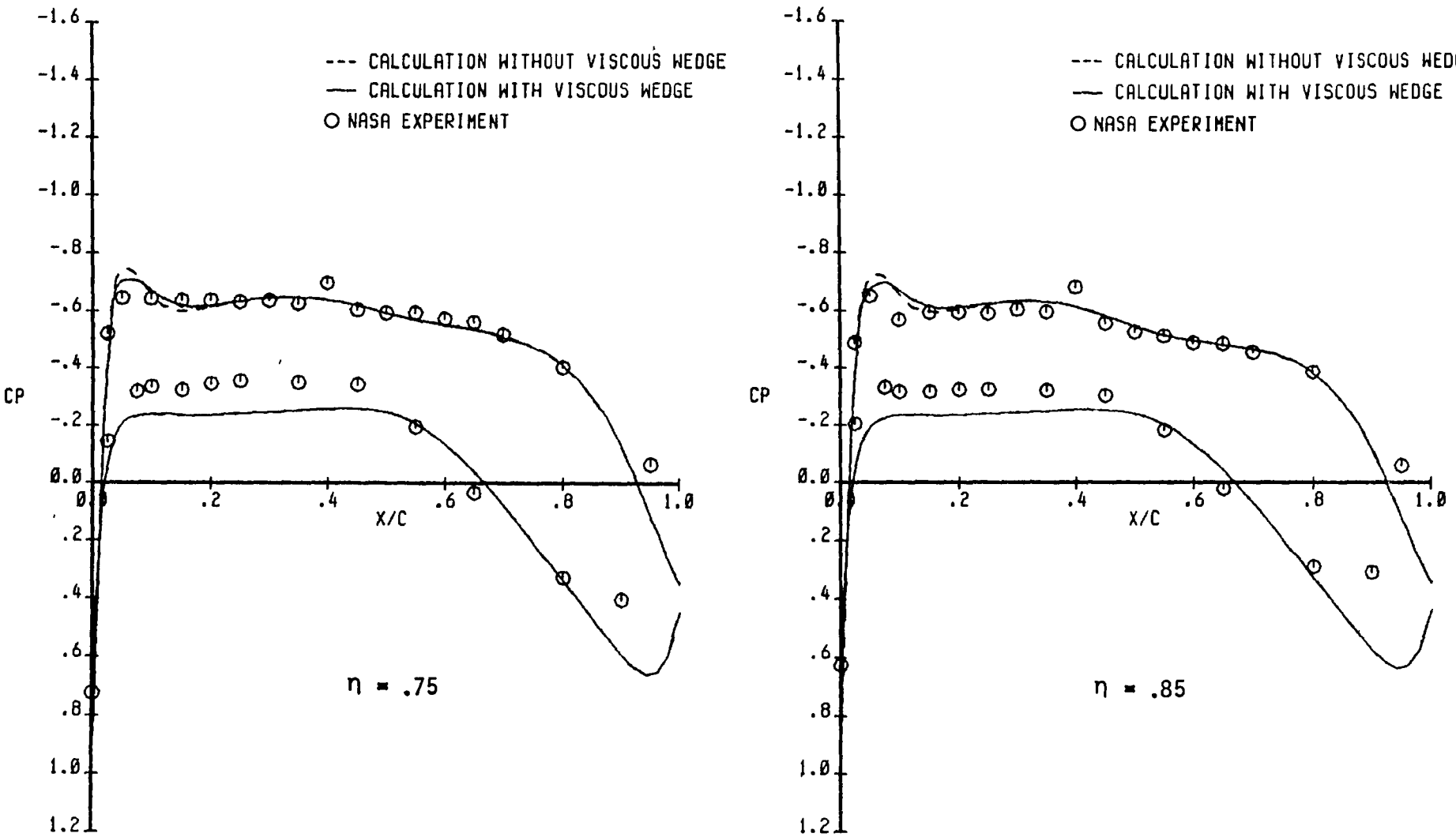

Figure 4 Continued

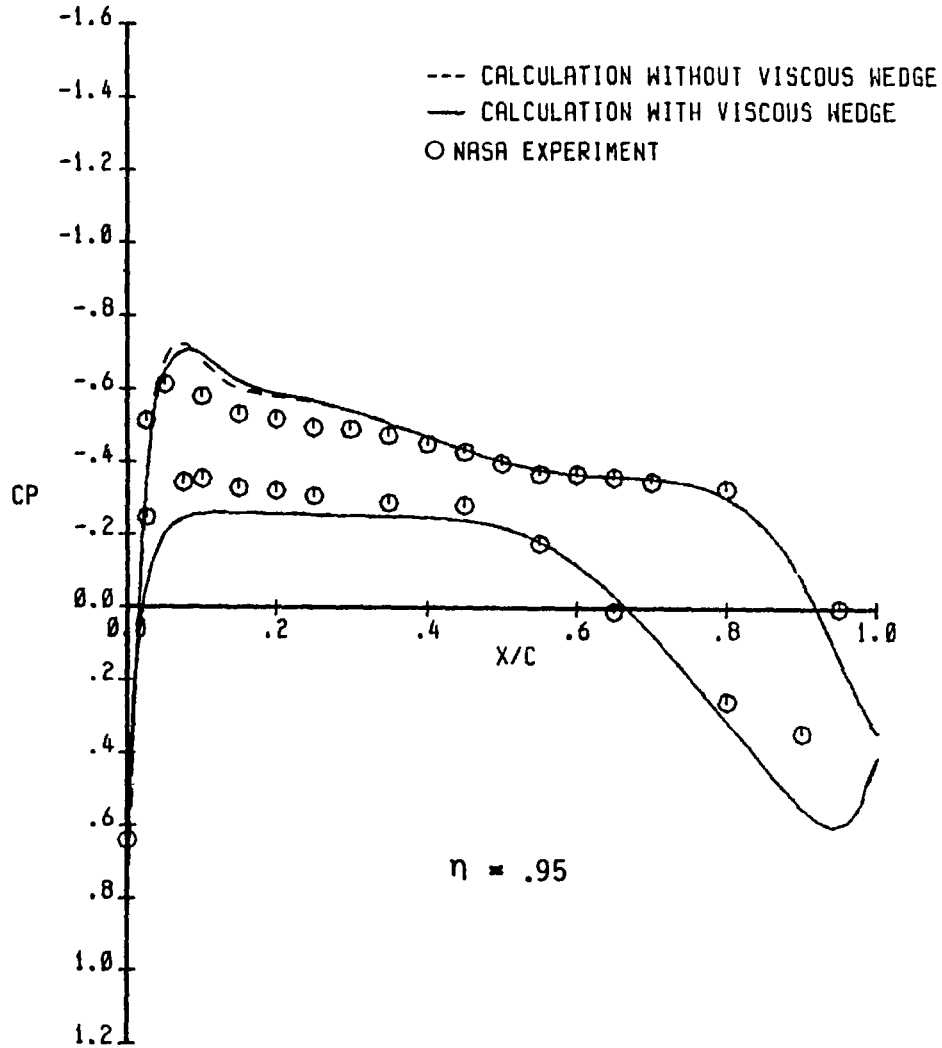

Figure 4 Concluded

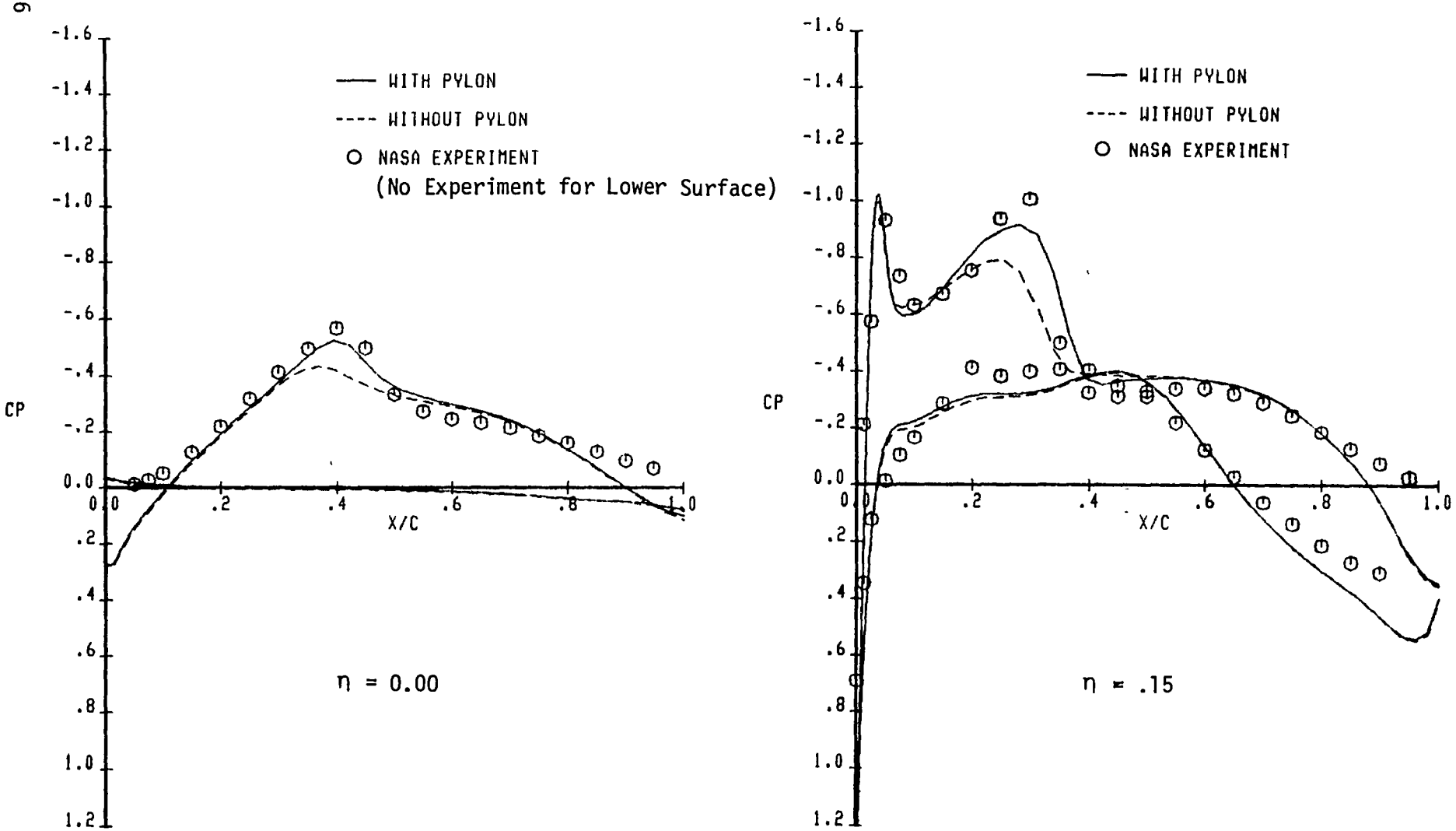

Figure 5 Pressure Distribution of the OTW Contoured Nacelle/Pylon Configuration
($M = 0.80$, $C_L = 0.45$)

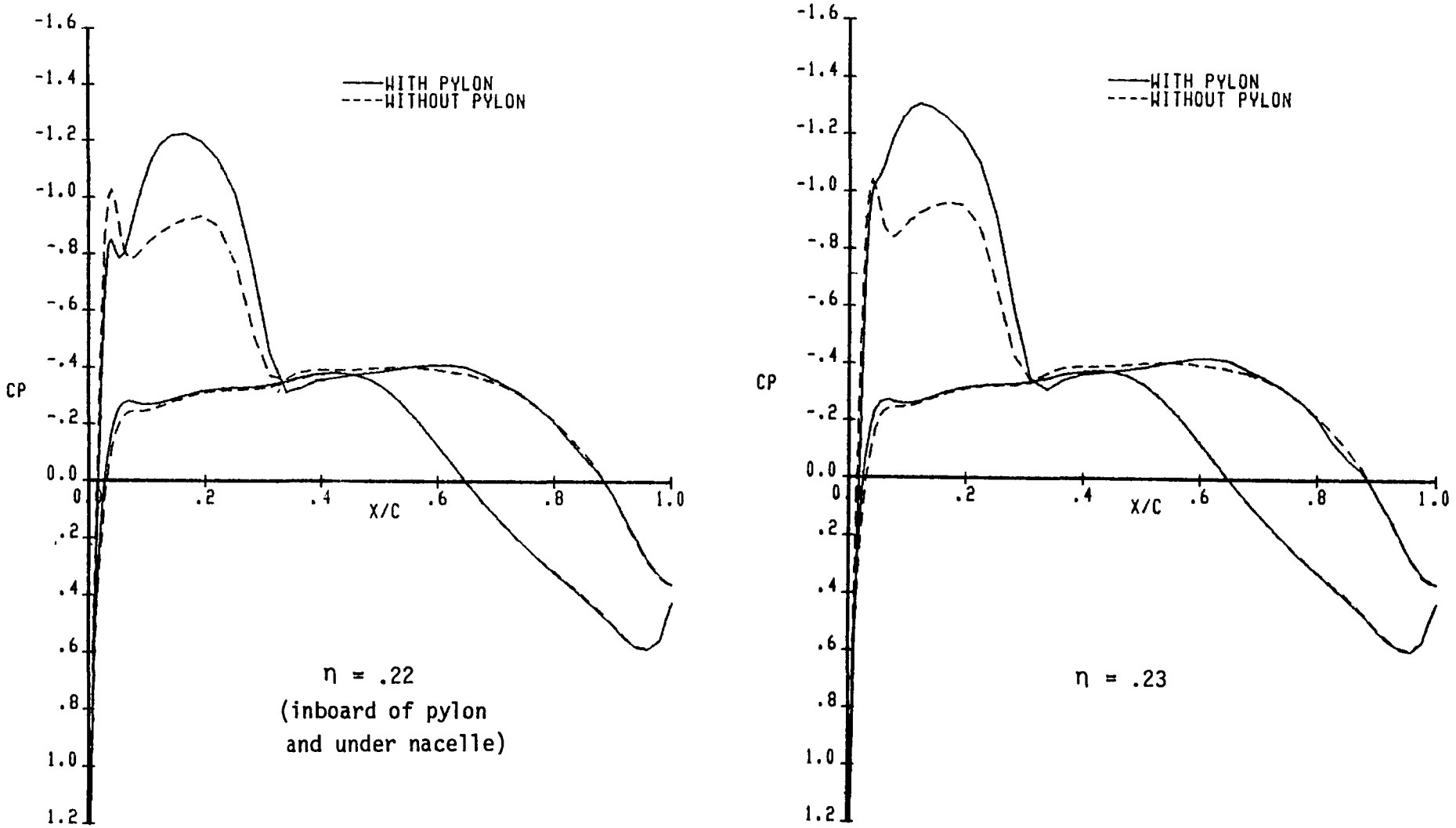

Figure 5 Continued

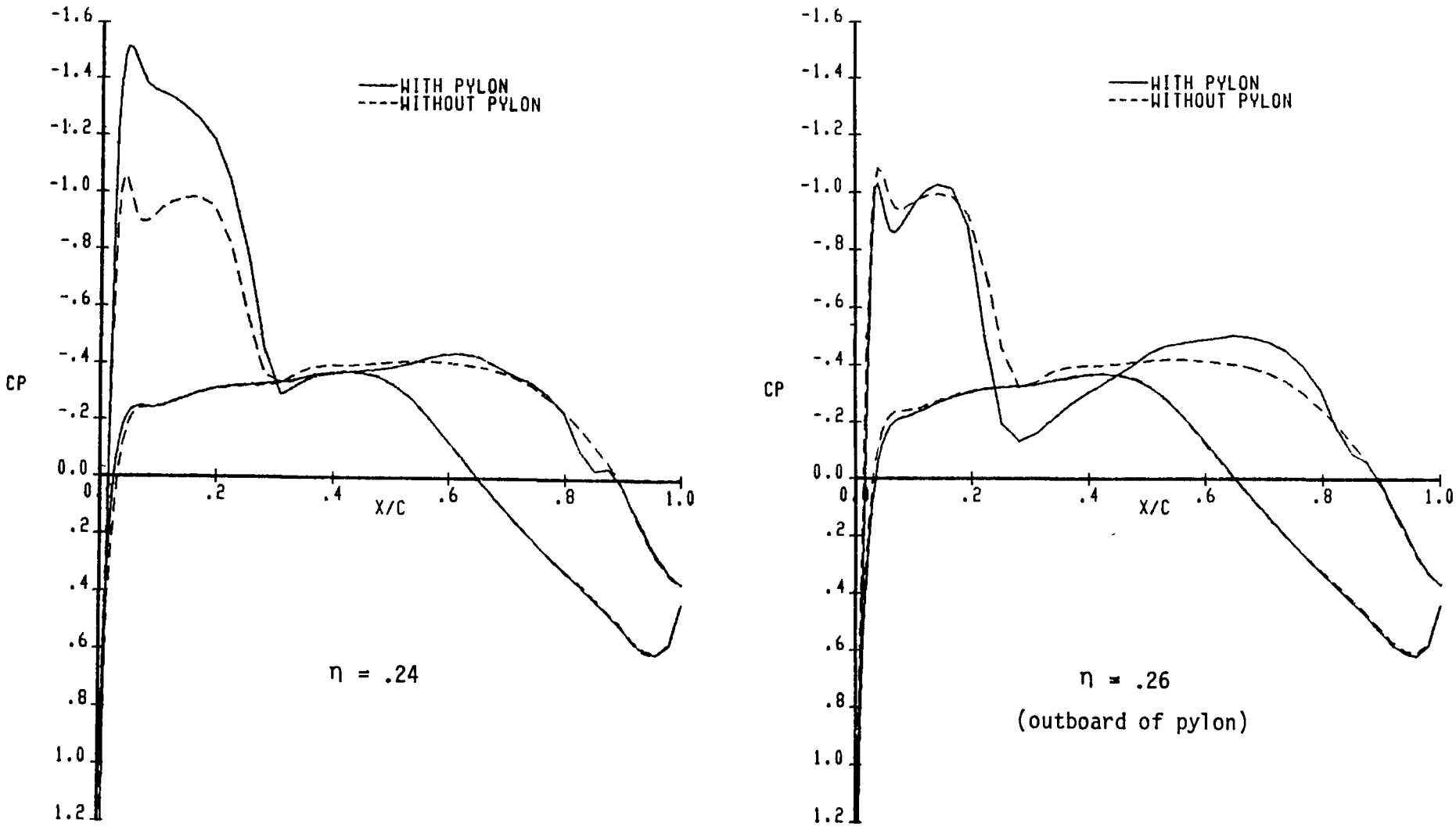

Figure 5 Continued

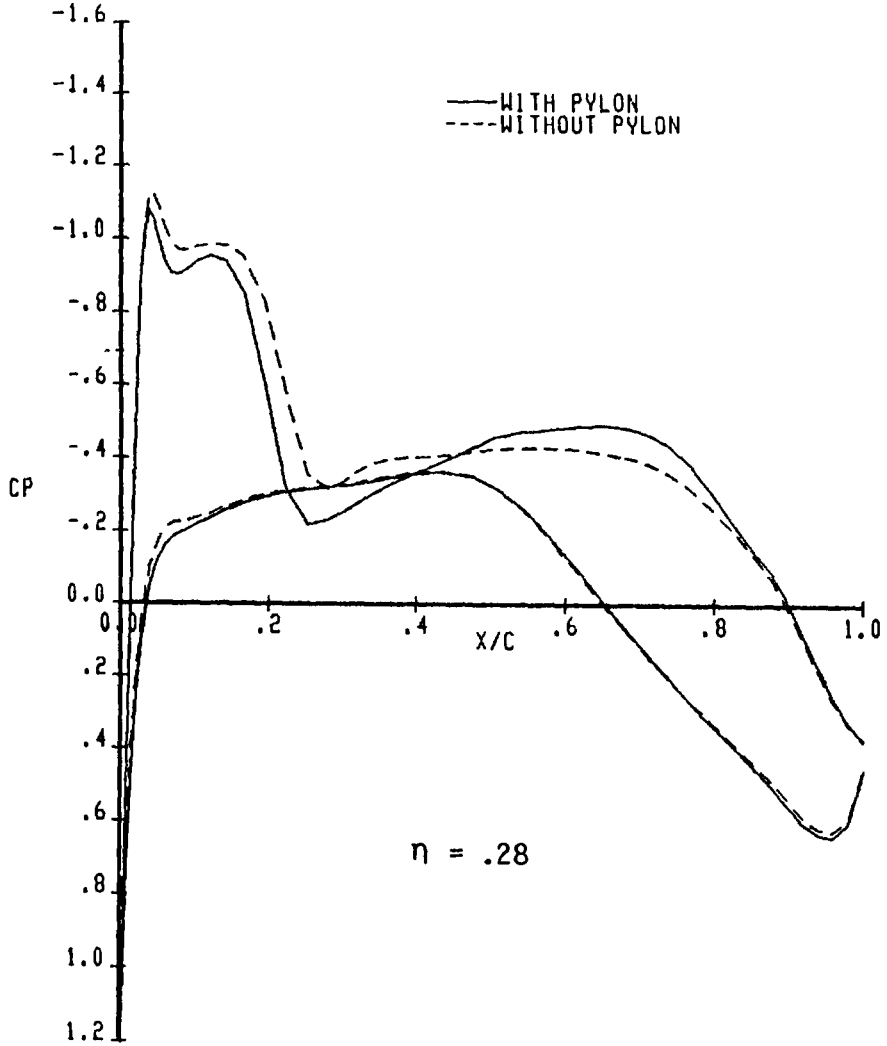

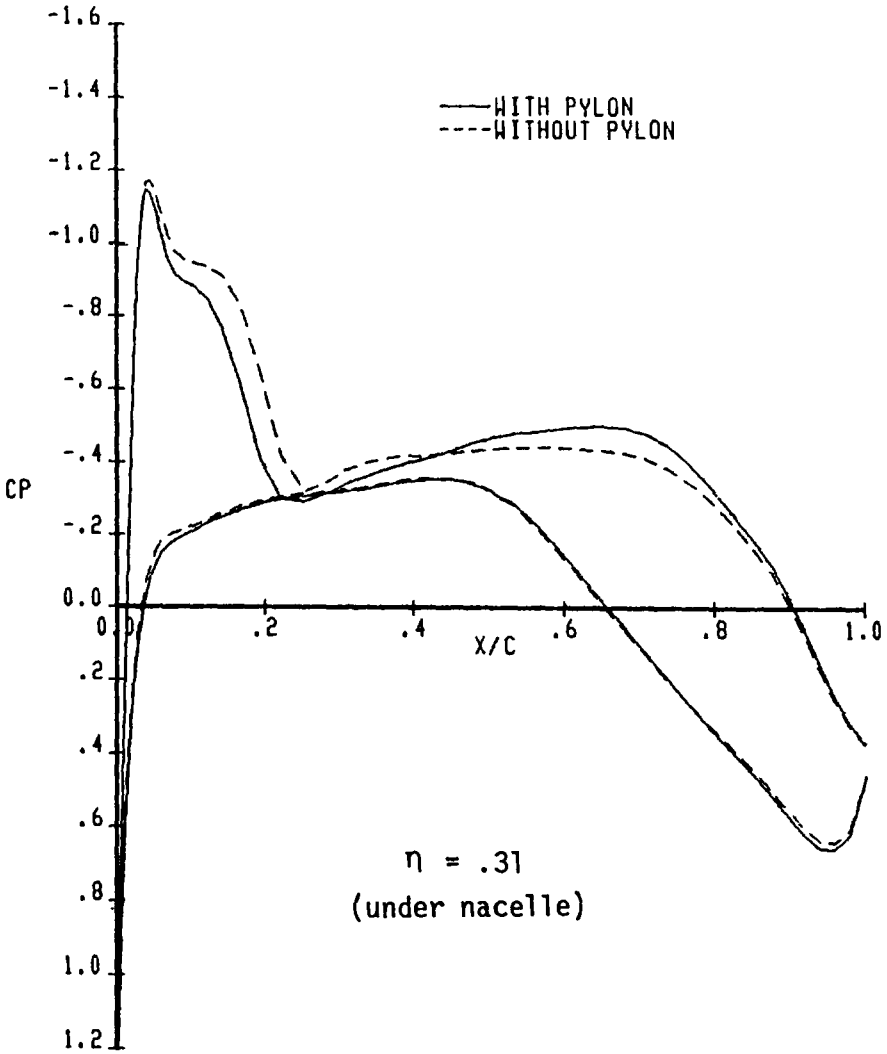

Figure 5 Continued

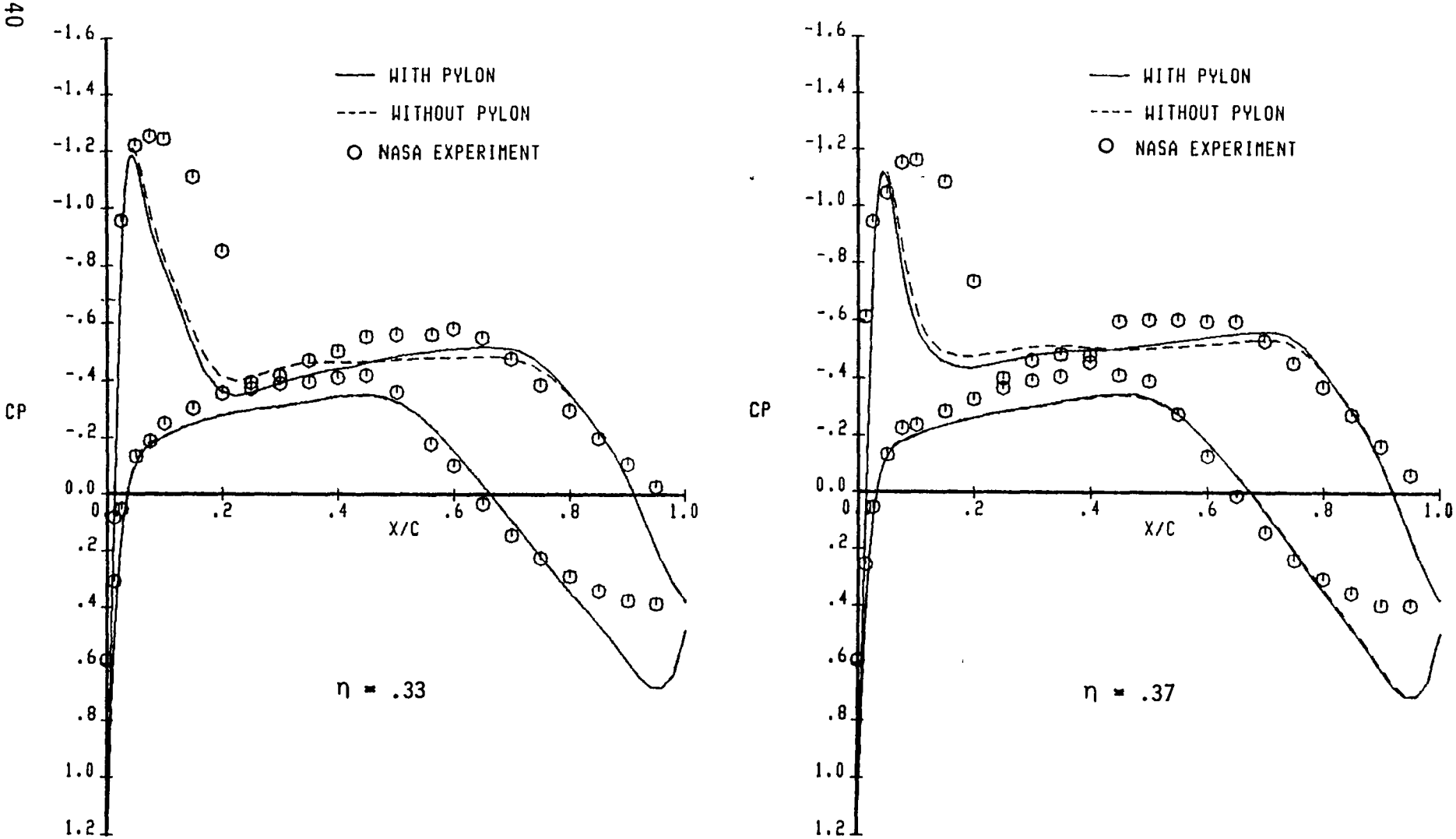

Figure 5 Continued

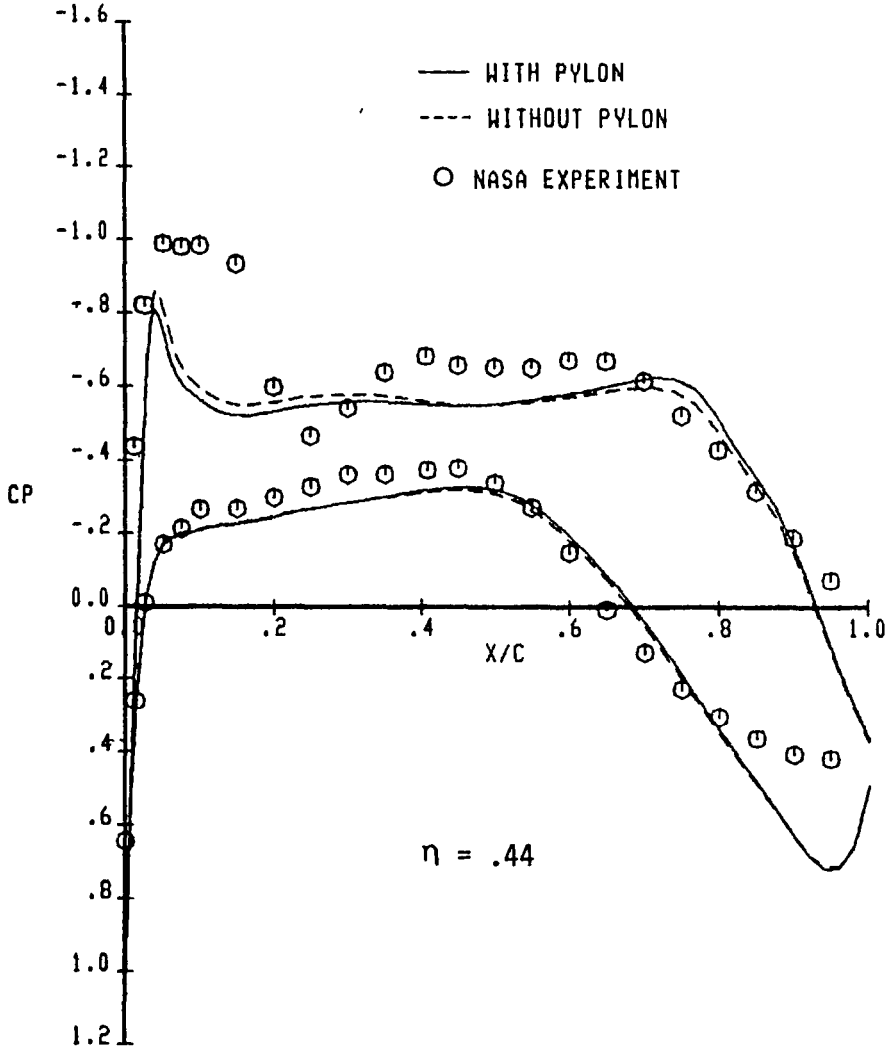

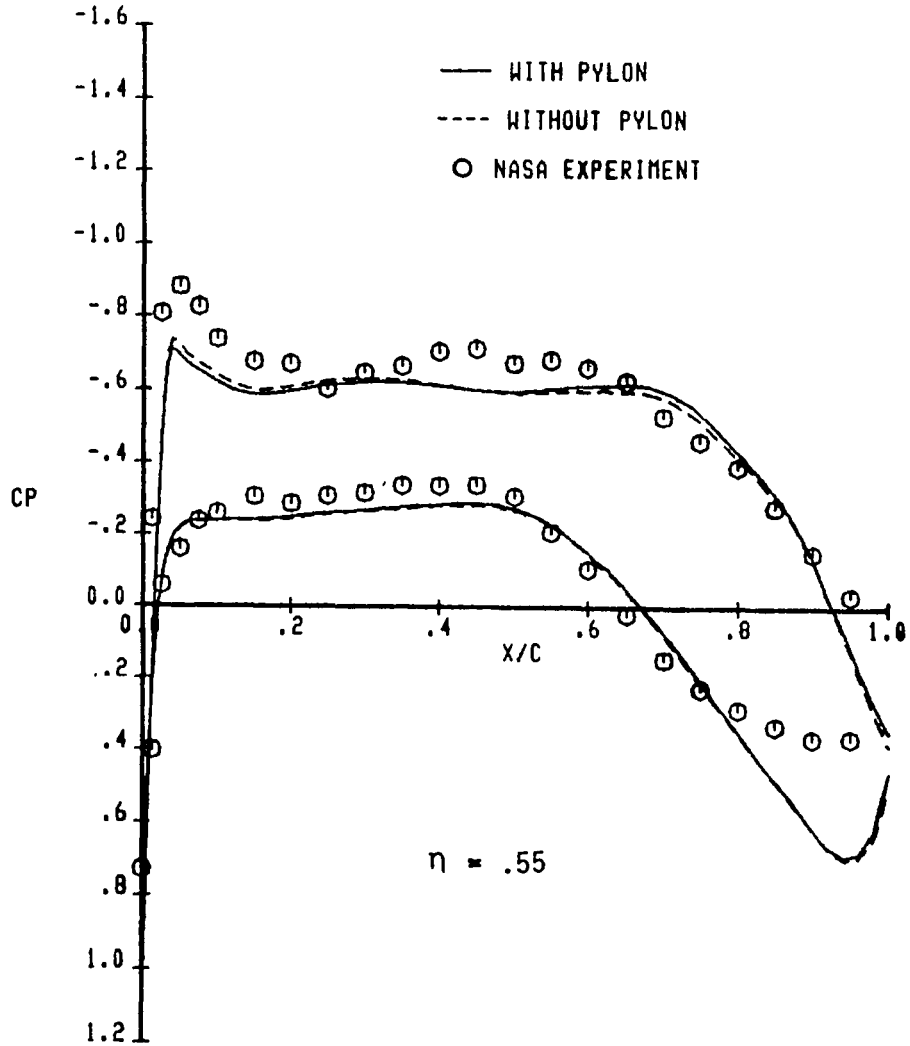

Figure 5 Concluded

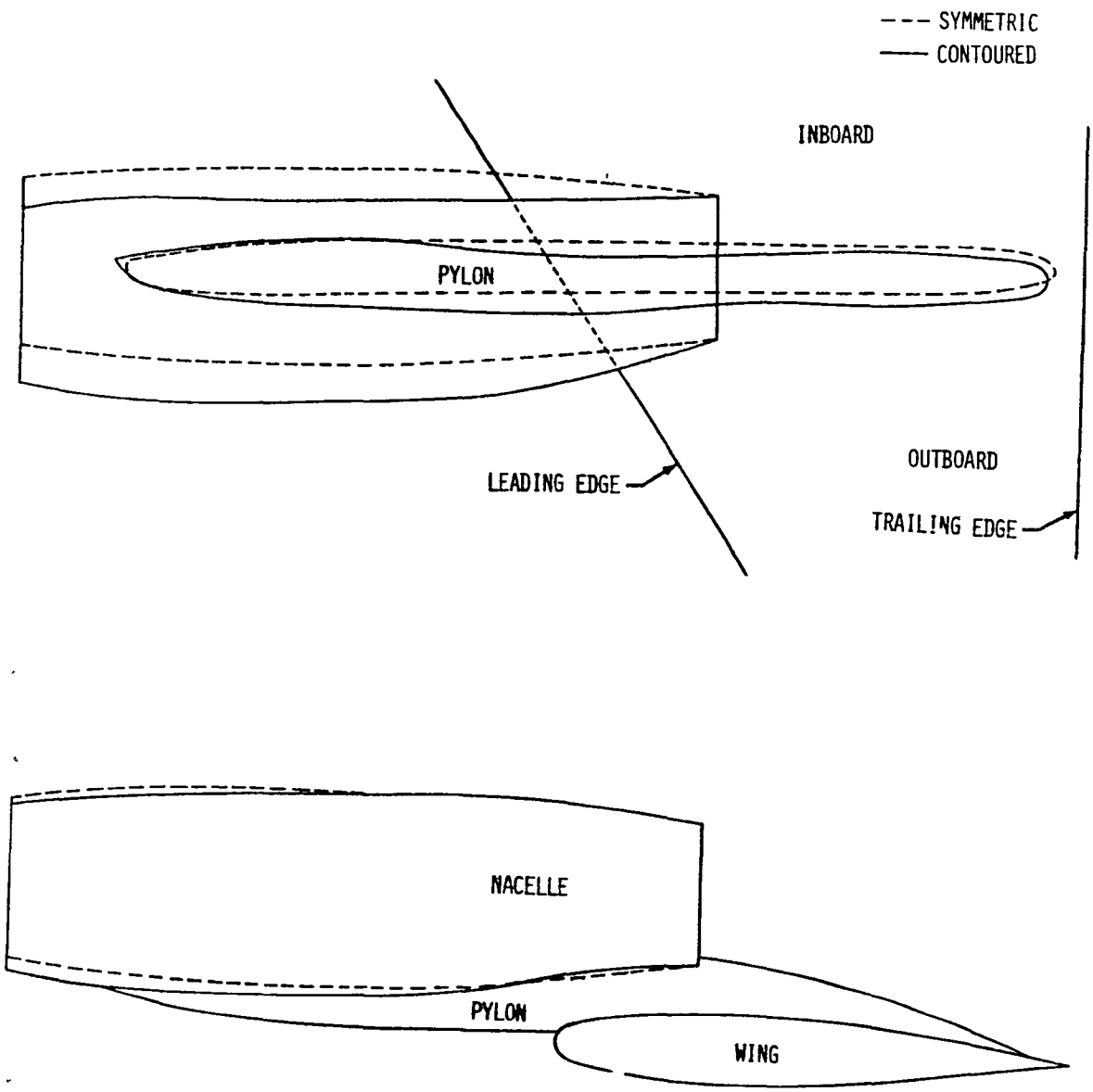

Figure 6 Comparison of the OTW Symmetric and Contoured Configurations

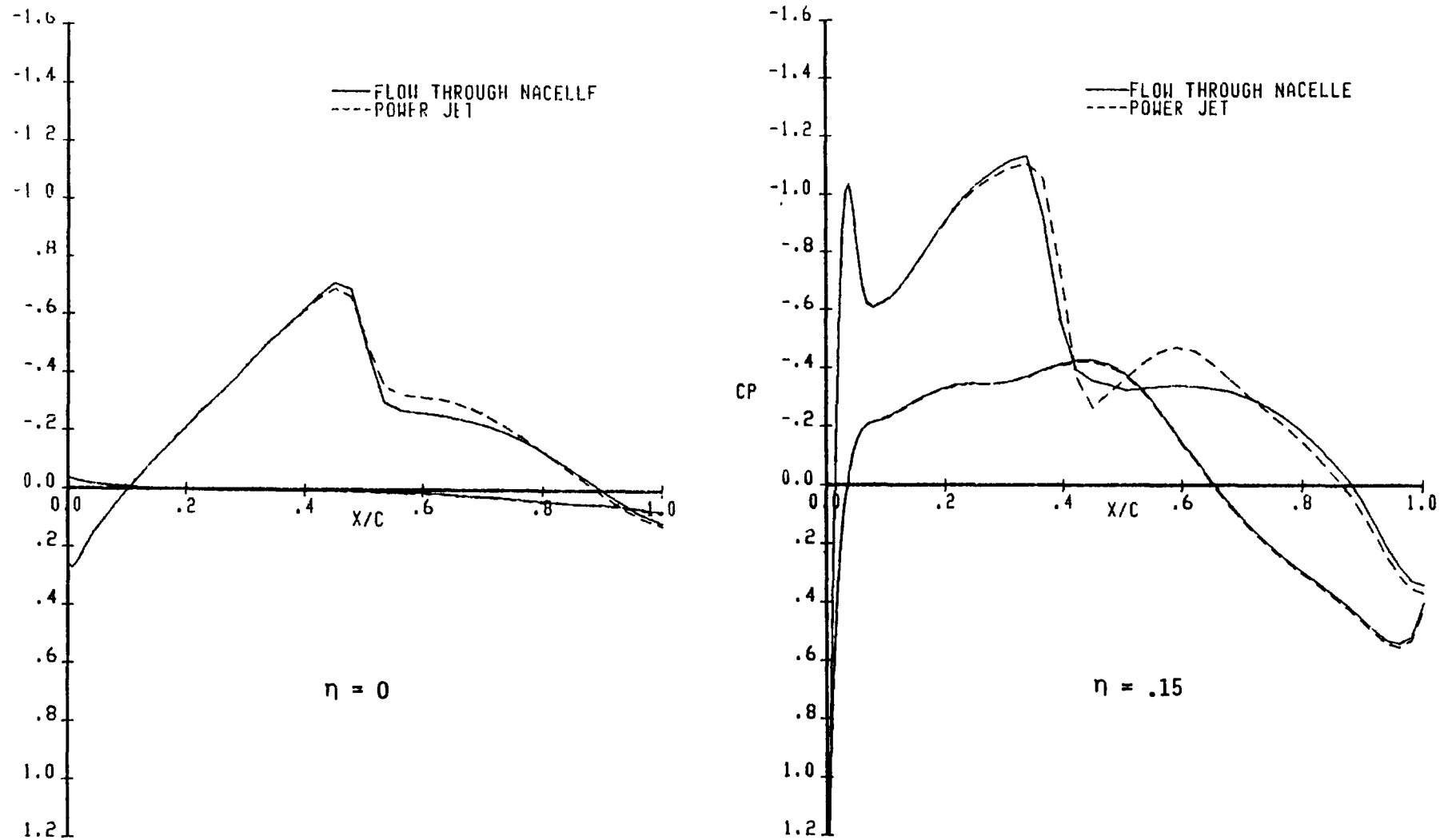

Figure 7. Pressure Distribution of the OTW Symmetric Nacelle/Pylon Configuration in Flow Through and Power Jet modes ($M_\infty = 0.80$, $C_L = 0.45$)

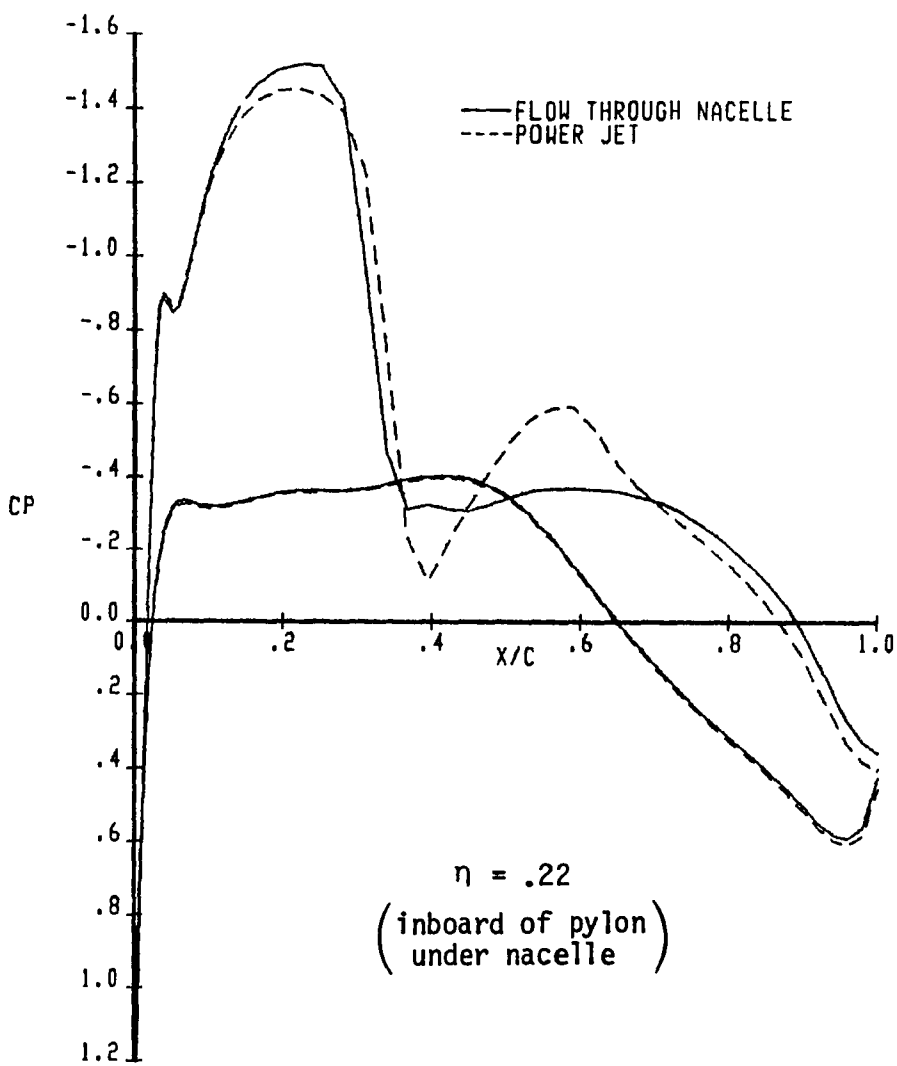

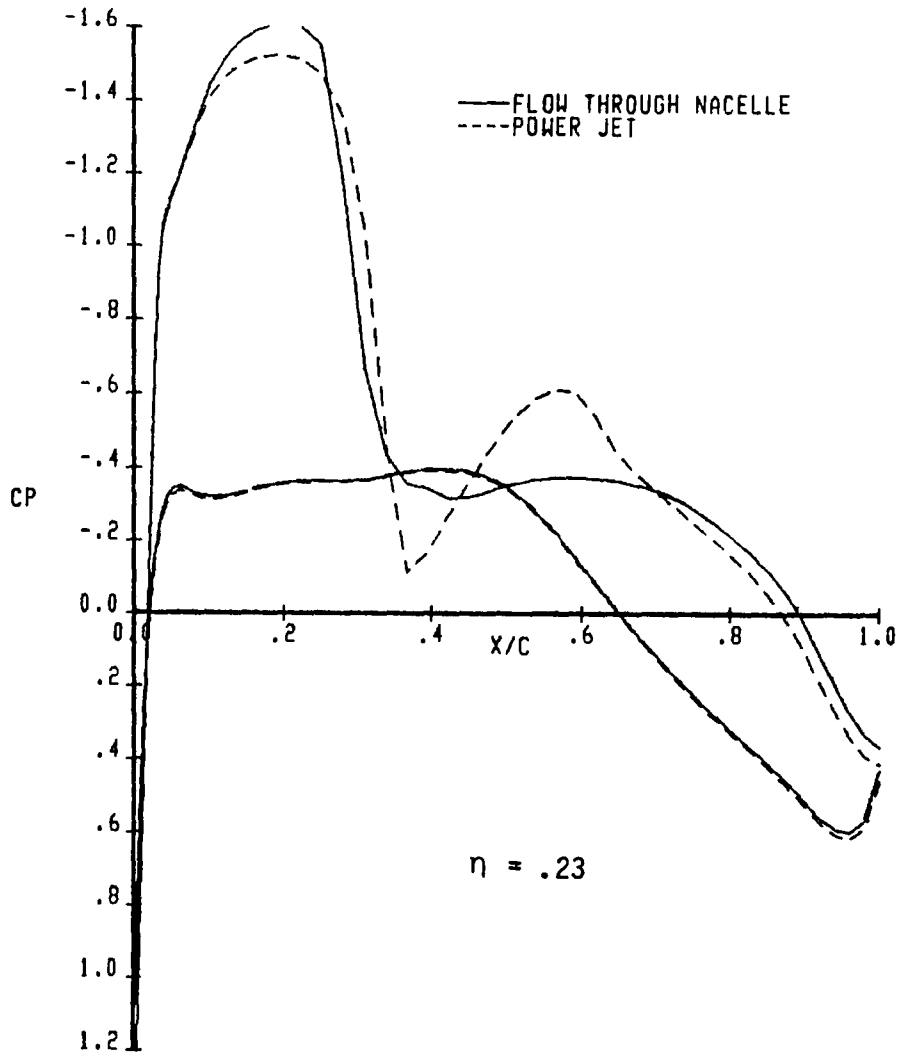

Figure 7 Continued

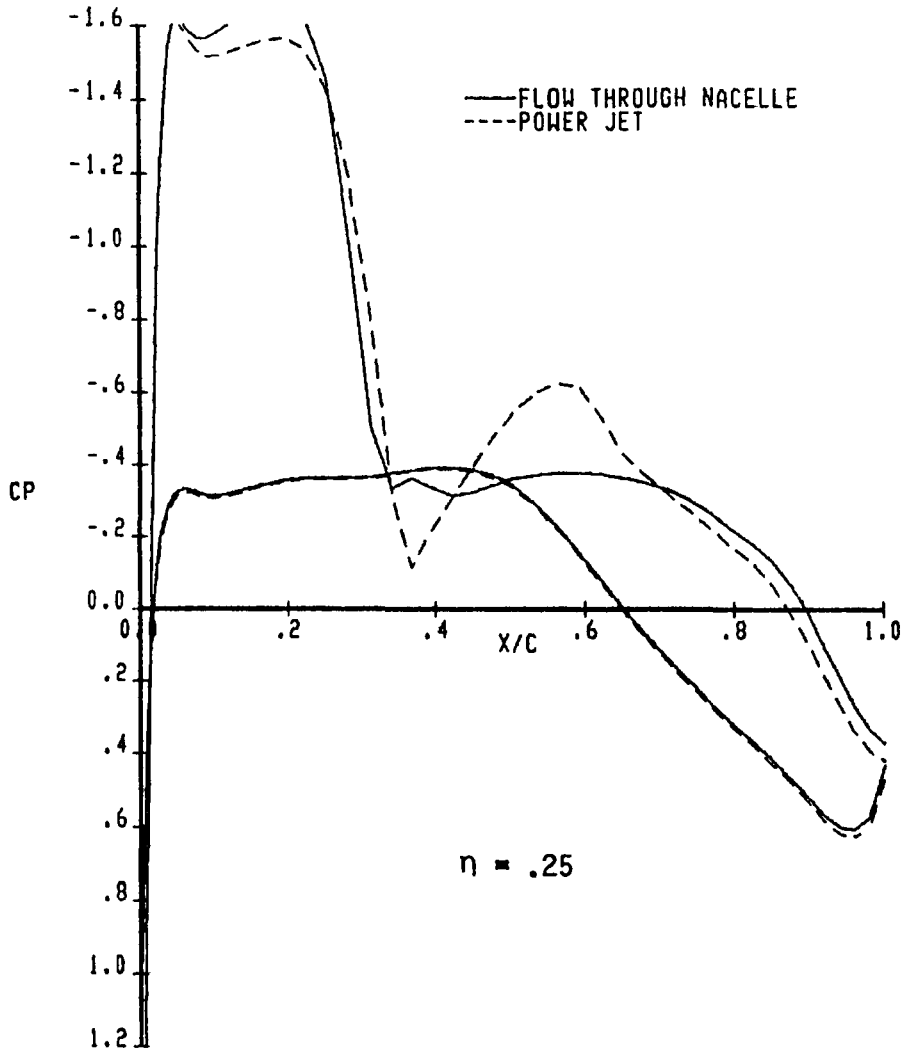

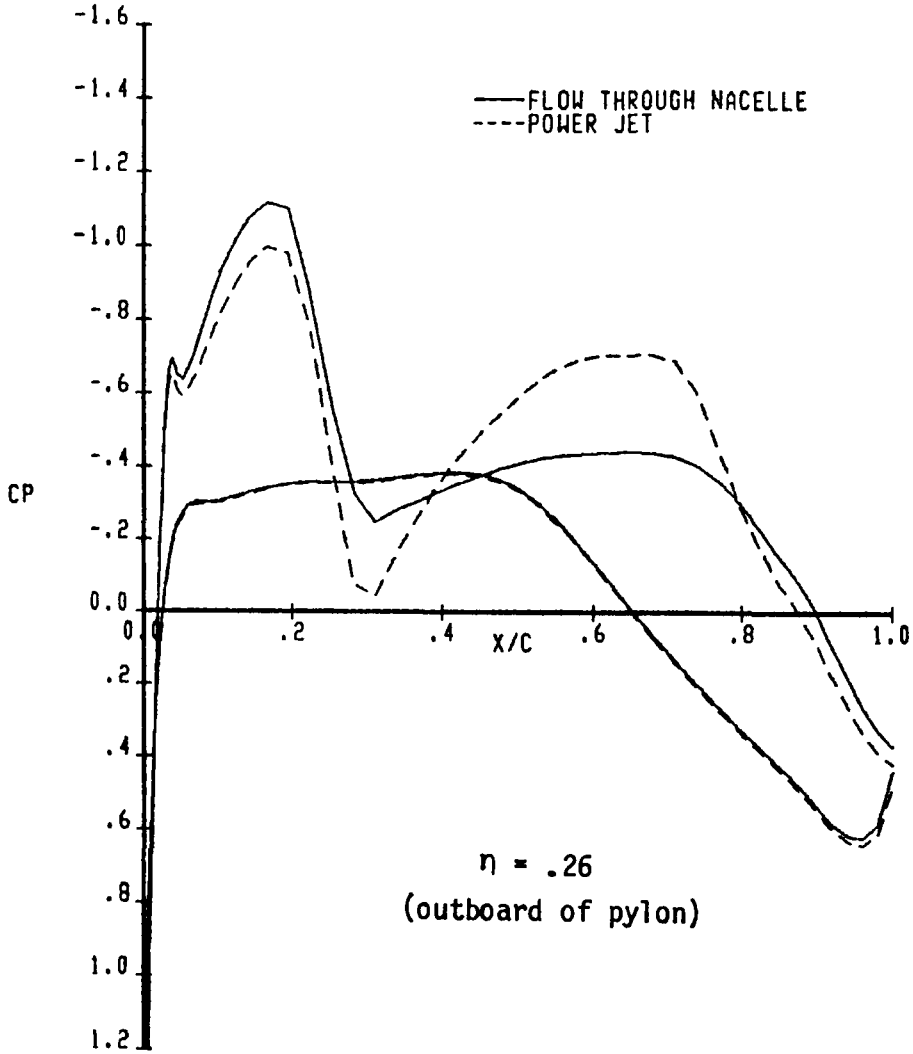

Figure 7 Continued

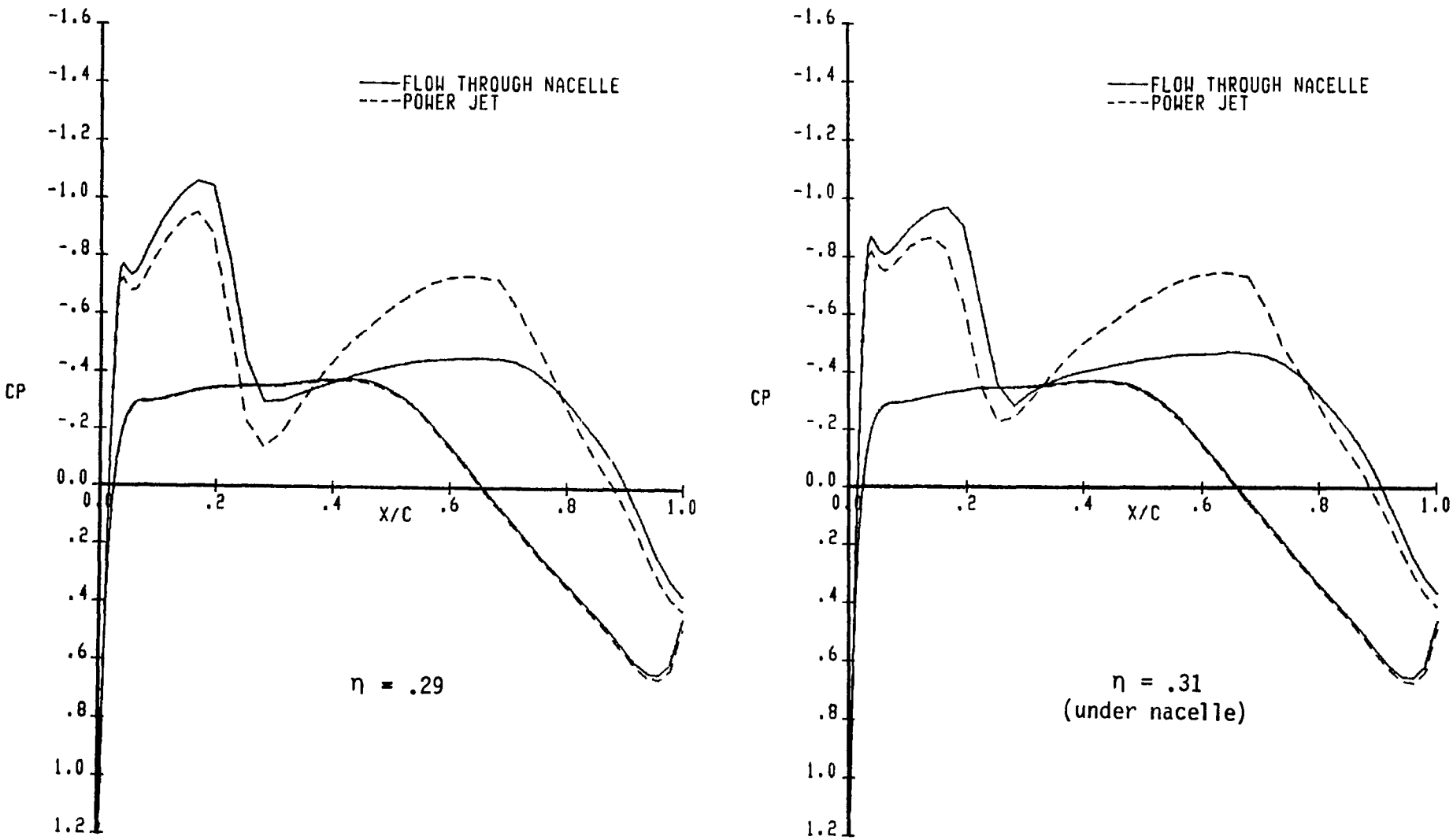

Figure 7 Continued

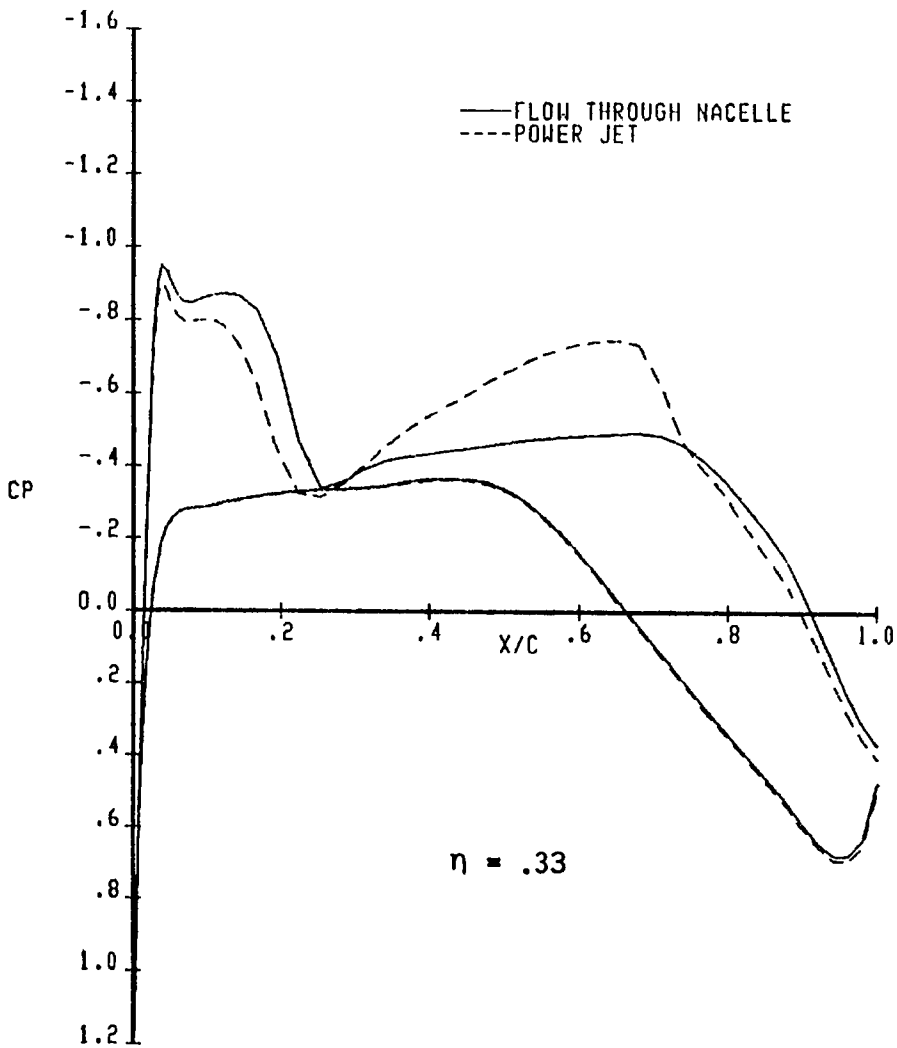

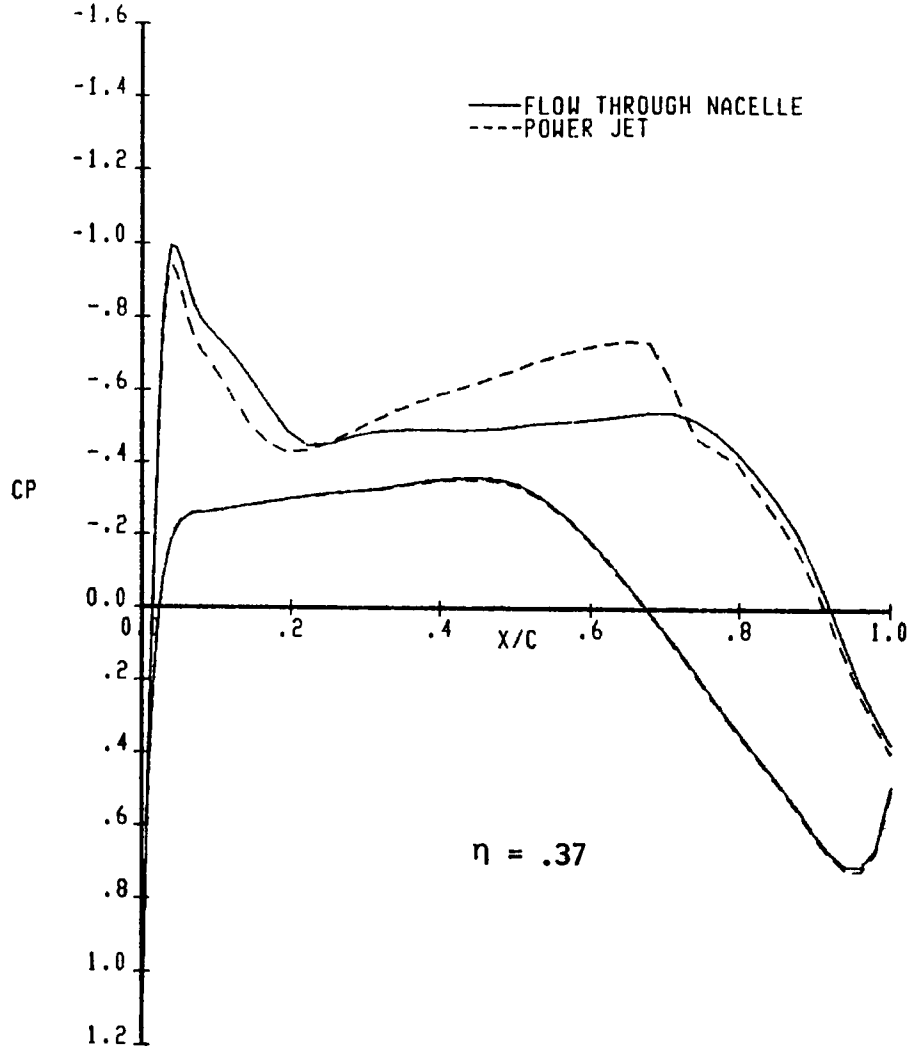

Figure 7 Continued

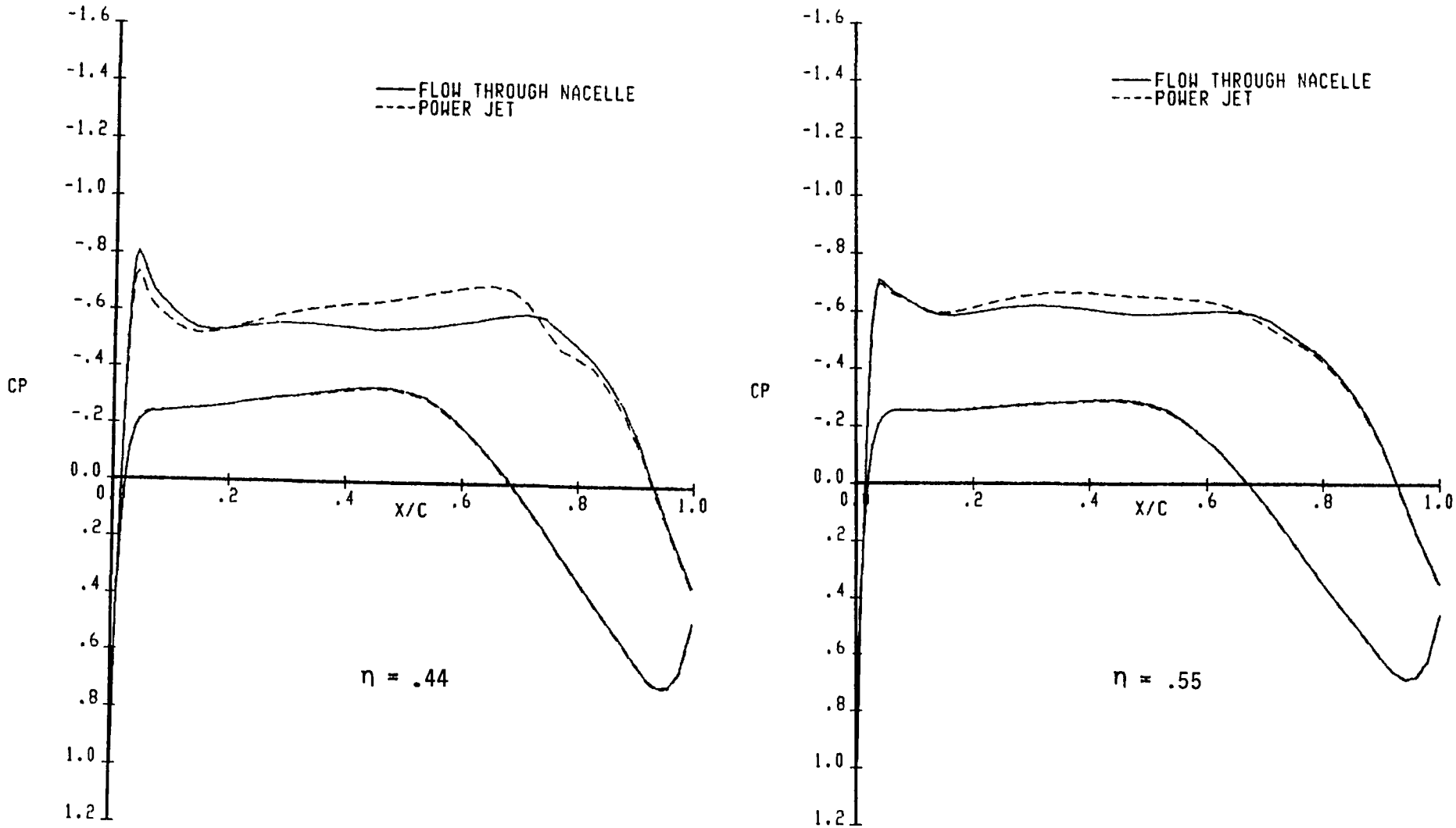

Figure 7 Continued

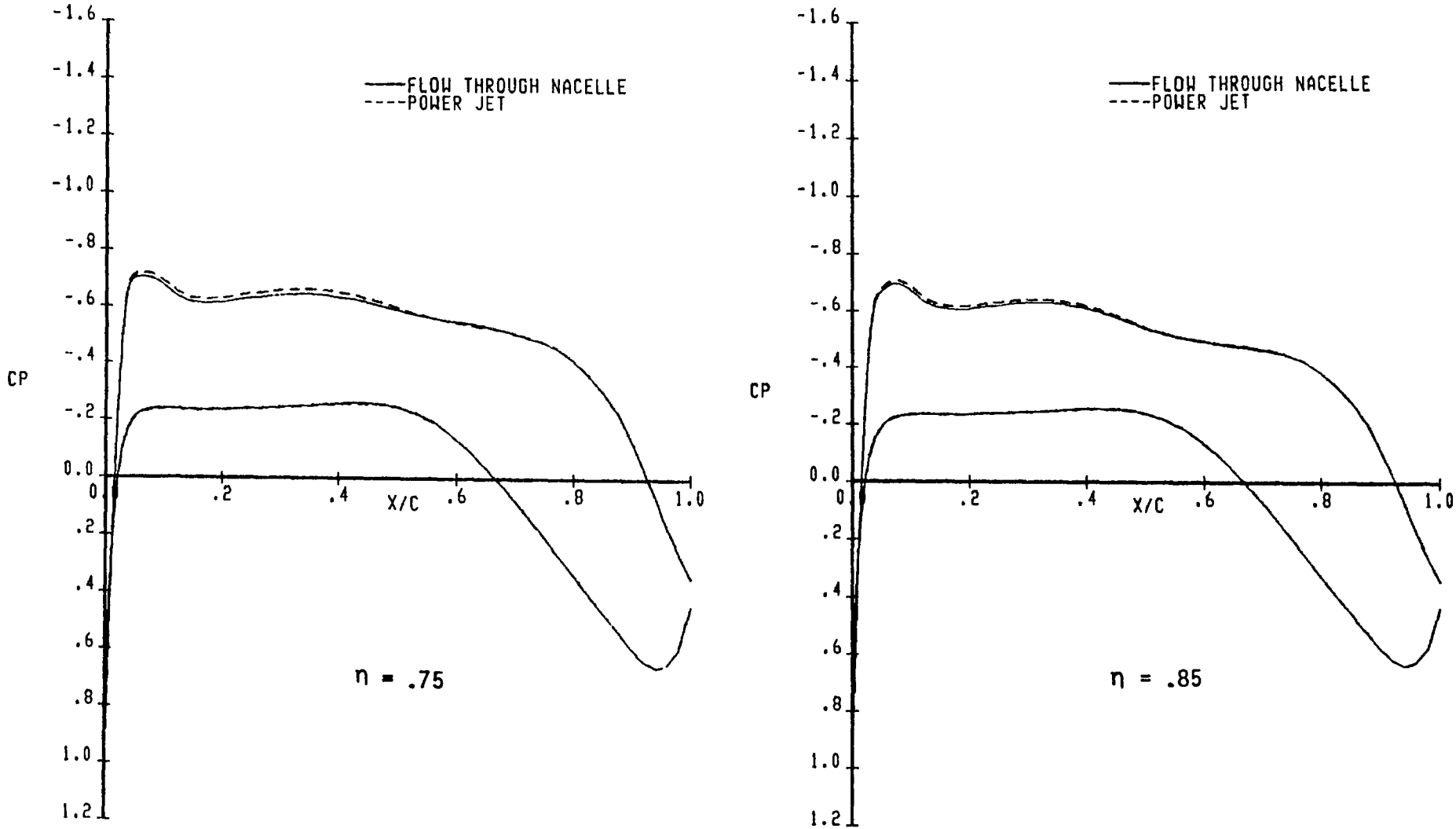

Figure 7 Concluded

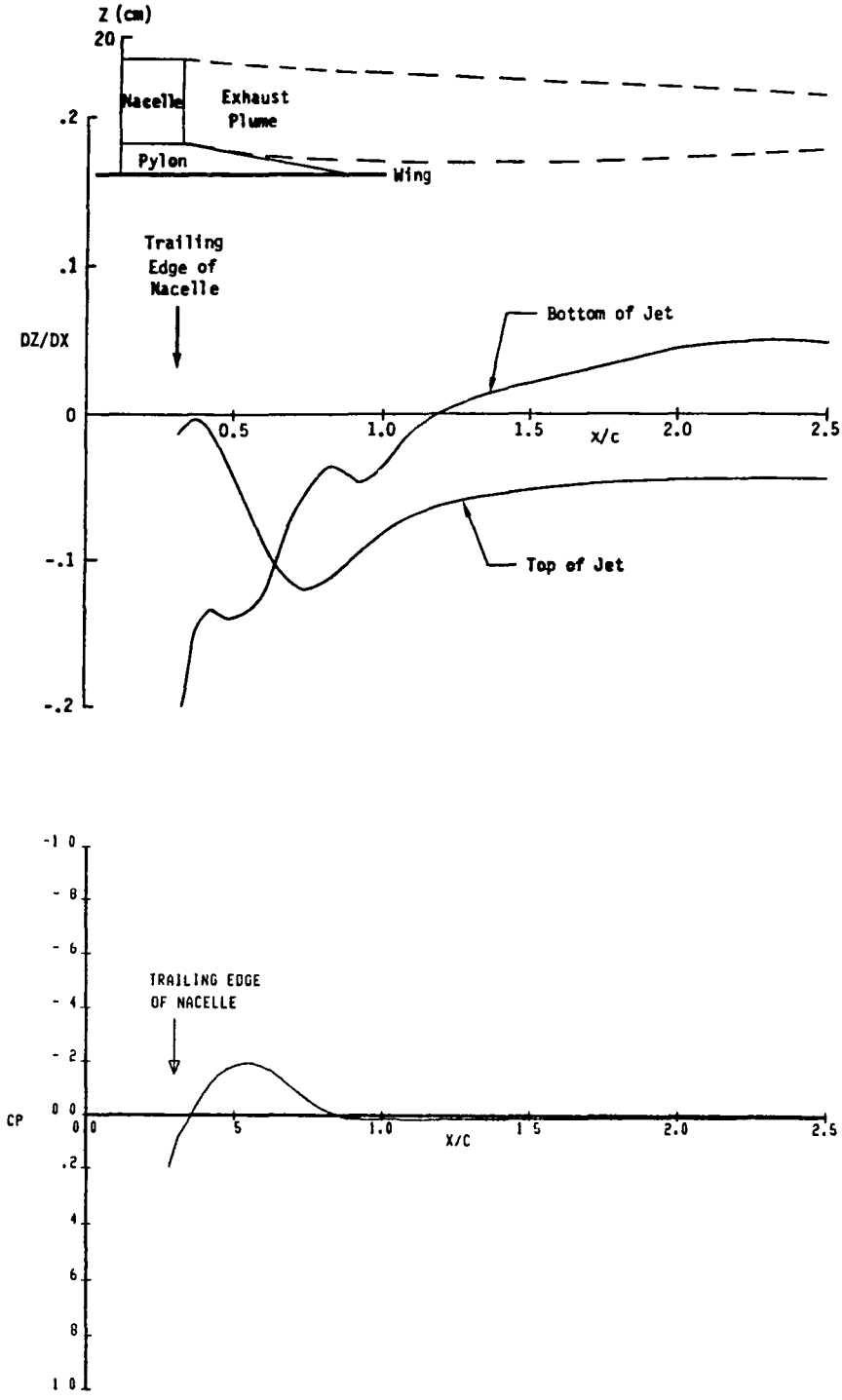

Figure 8 Plume Shape and Pressure Distribution at Center Line of OTW Symmetric Nacelle/Pylon Configuration

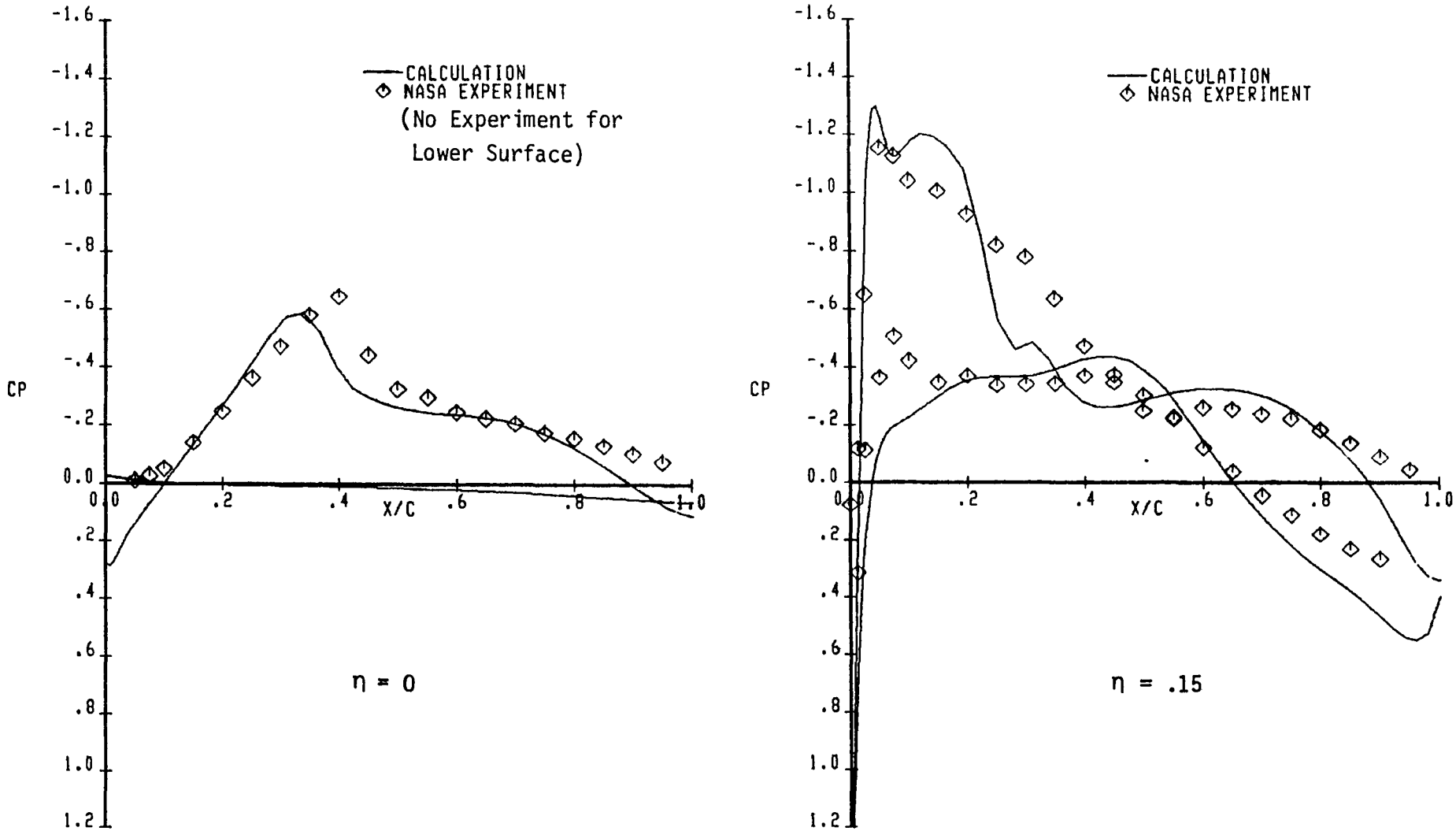

Figure 9. Pressure Distribution of the USB Configuration
(M_∞ = 0.80, C_L = 0.45)

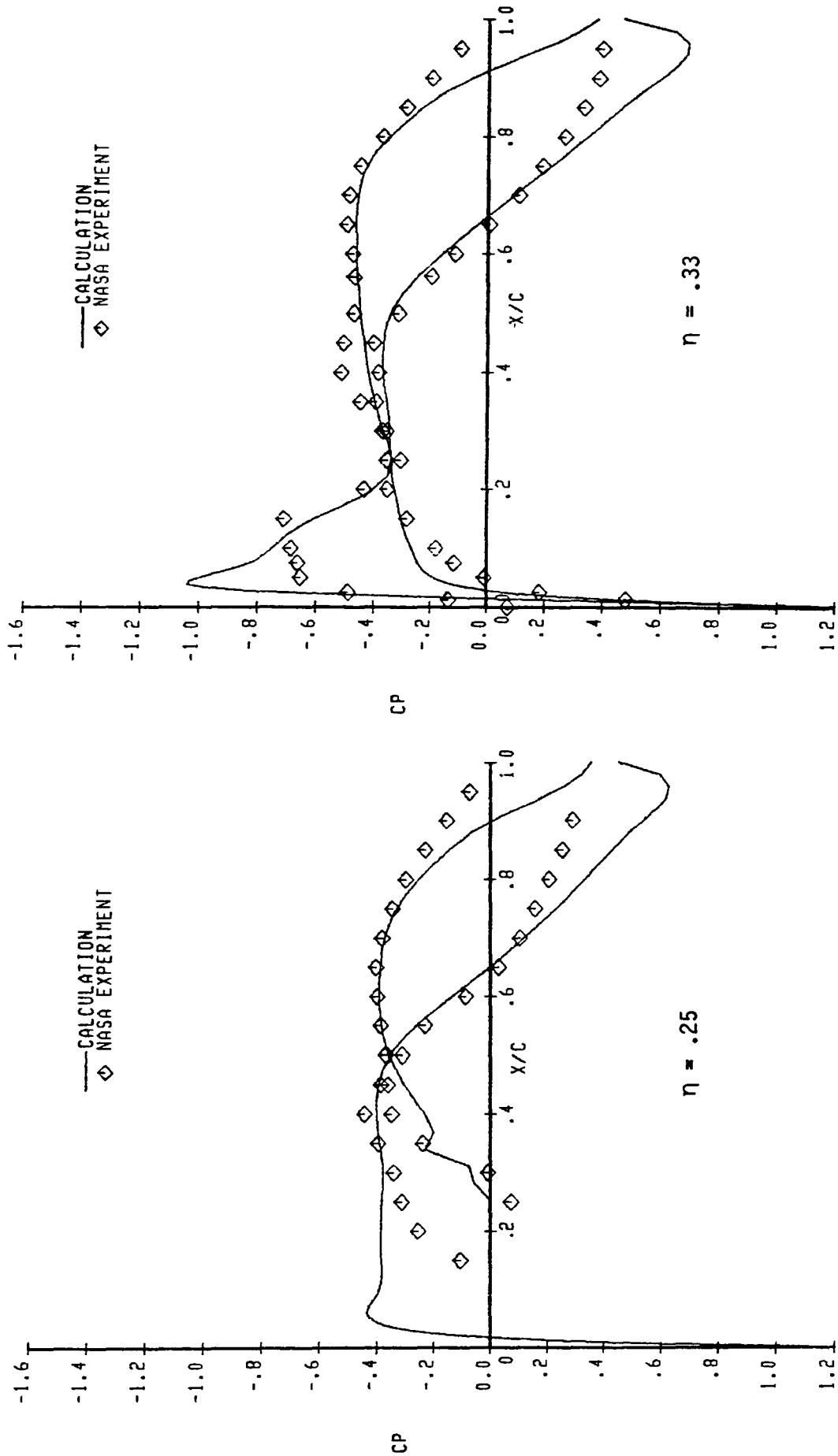

Figure 9 Continued

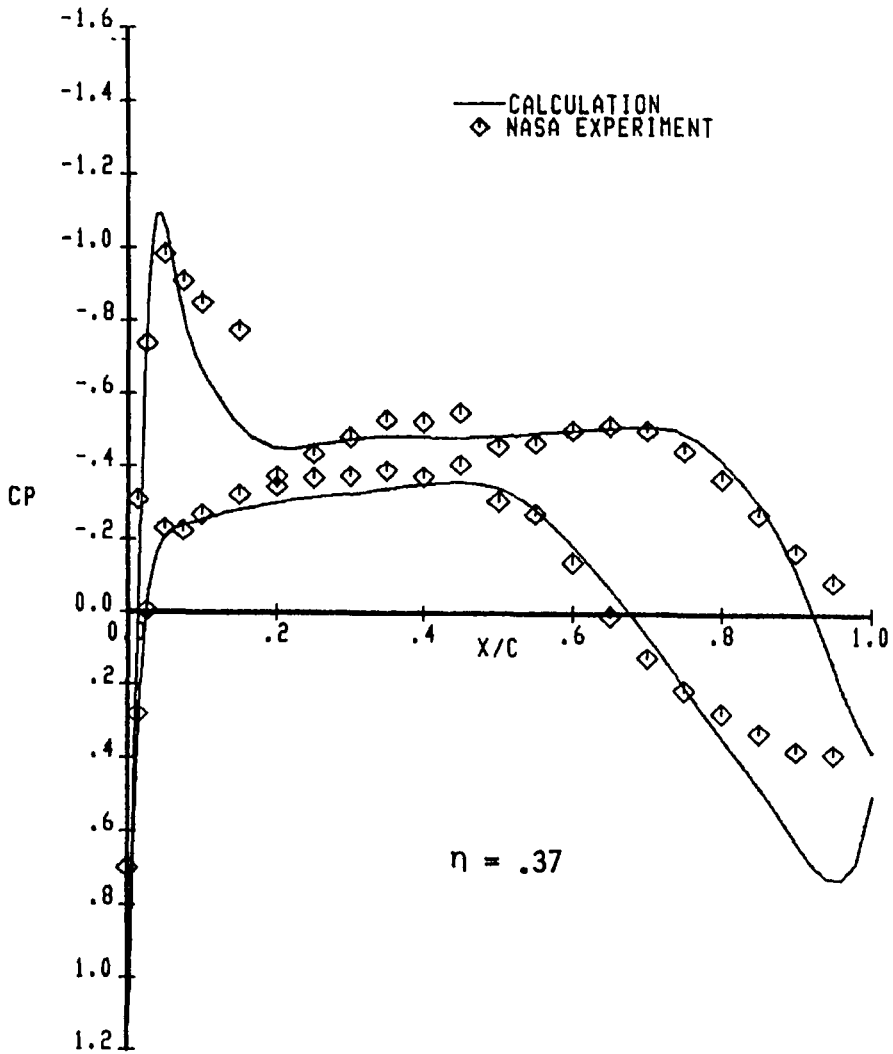

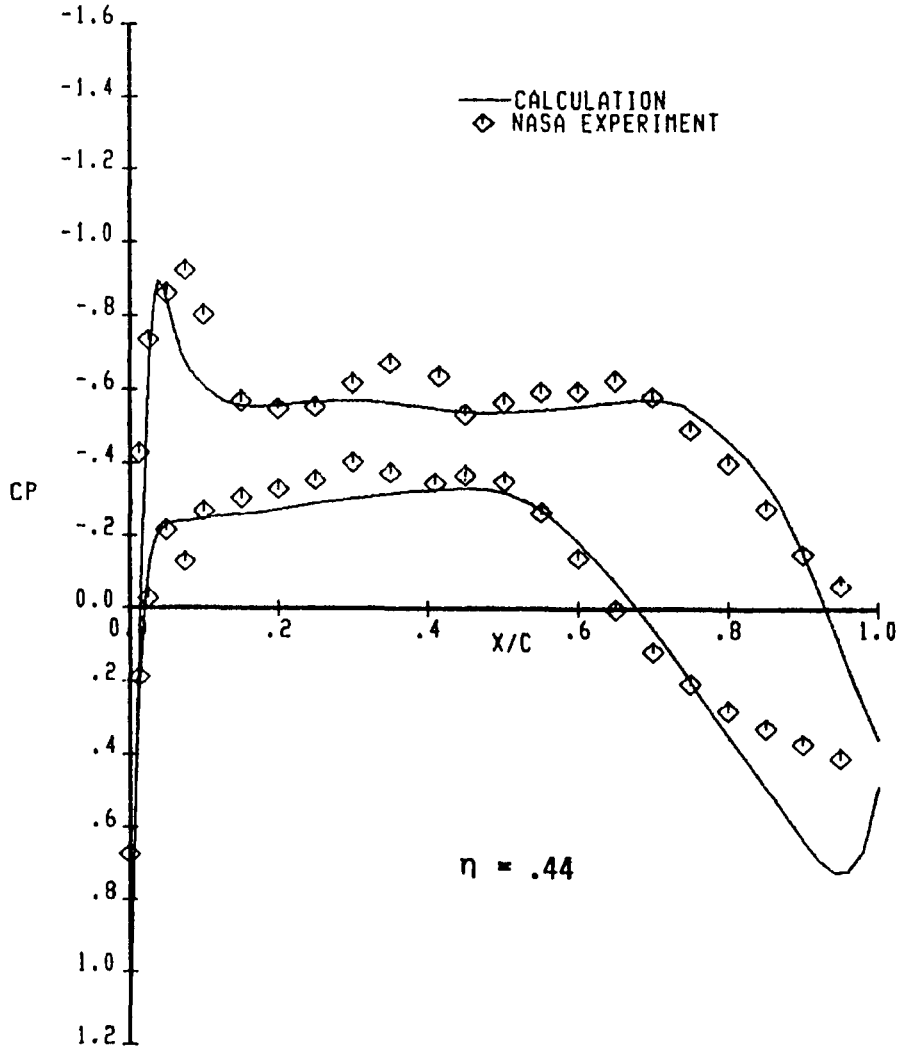

Figure 9 Continued

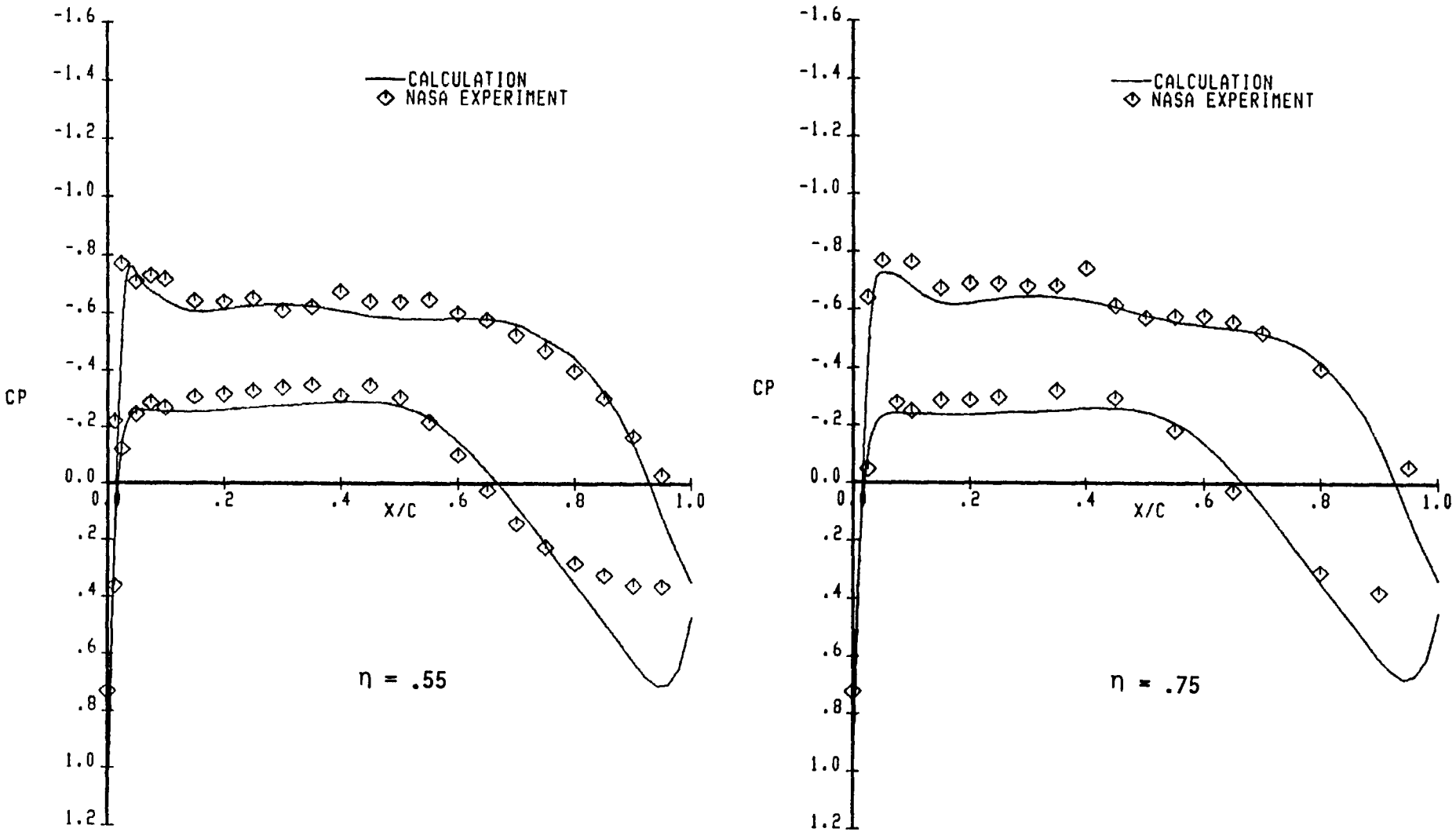

Figure 9 Continued

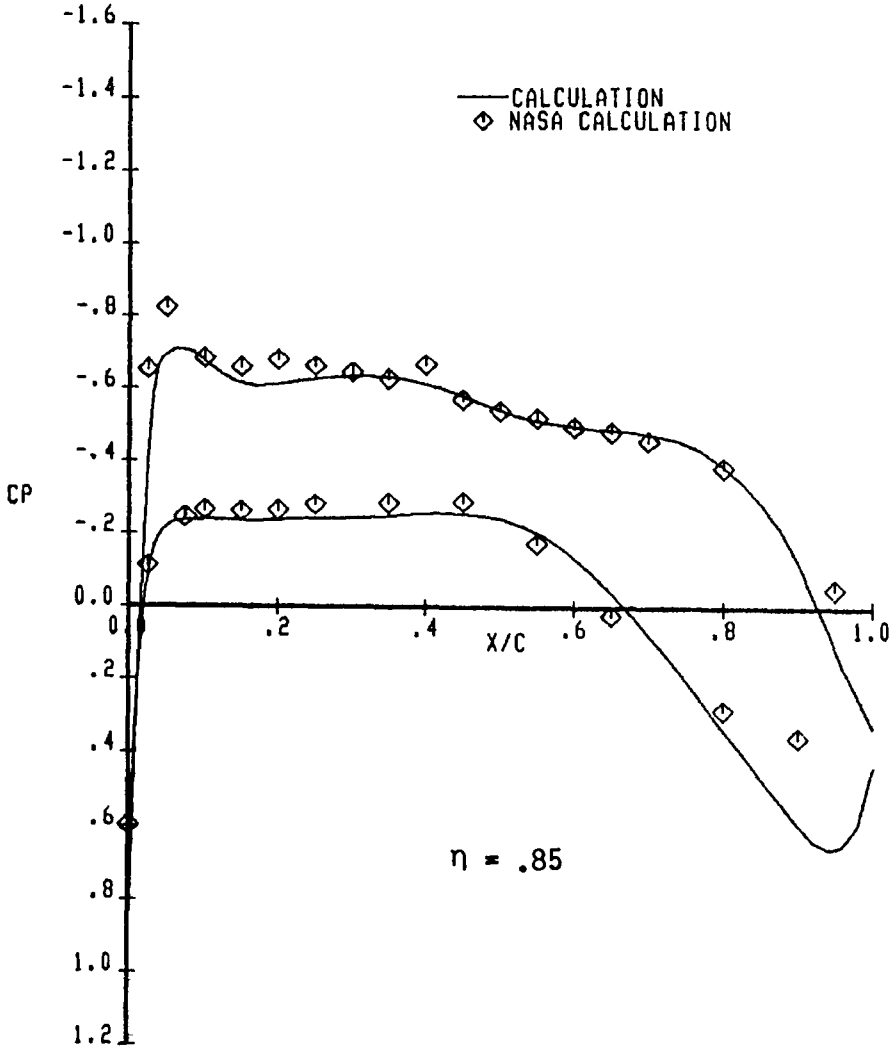

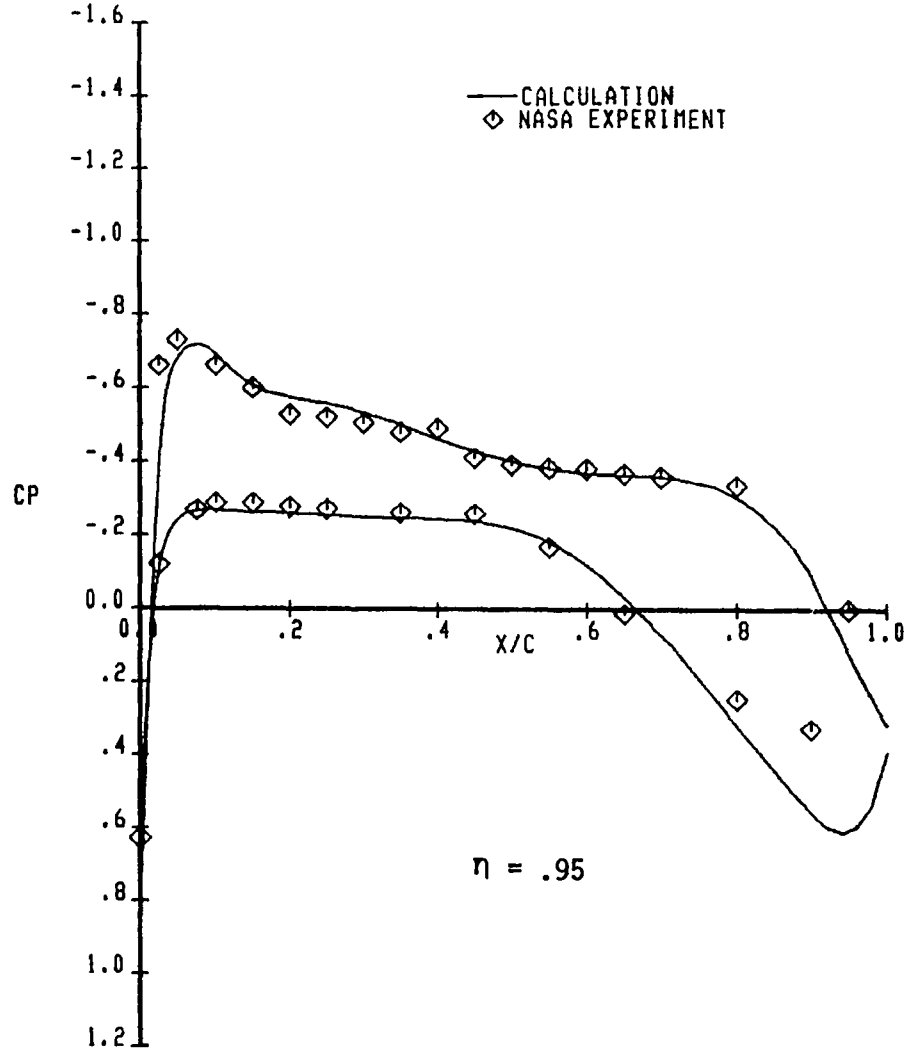

Figure 9 Concluded

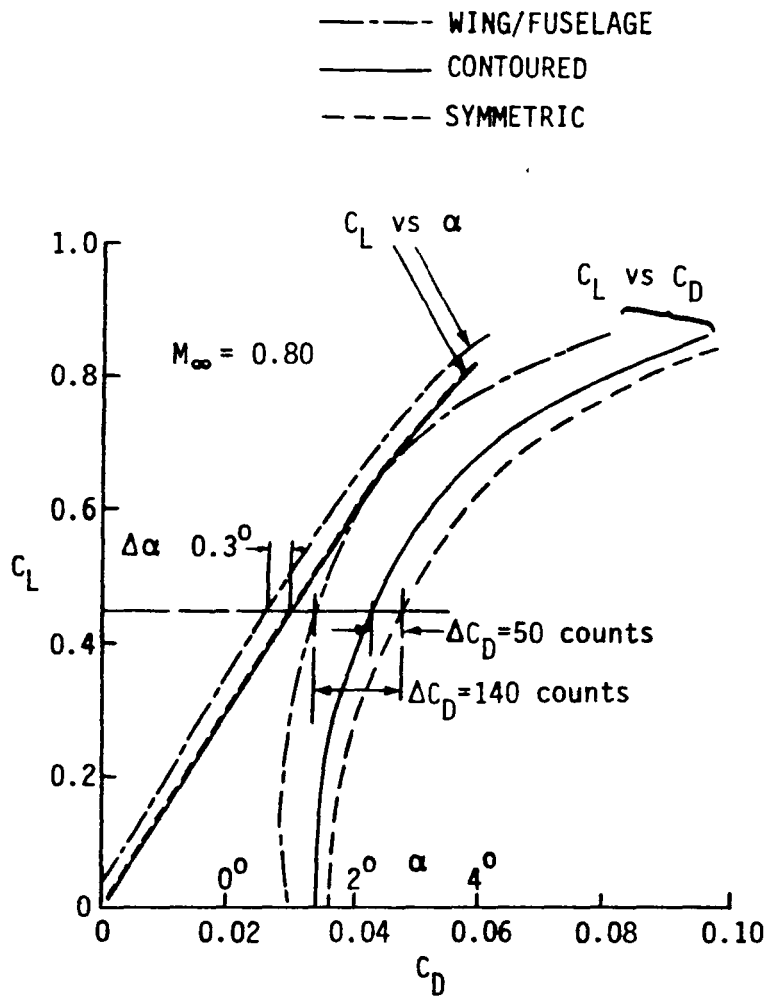

Figure 10 Measured Forces - Over-the-Wing Configuration (M_∞ = 0.80)

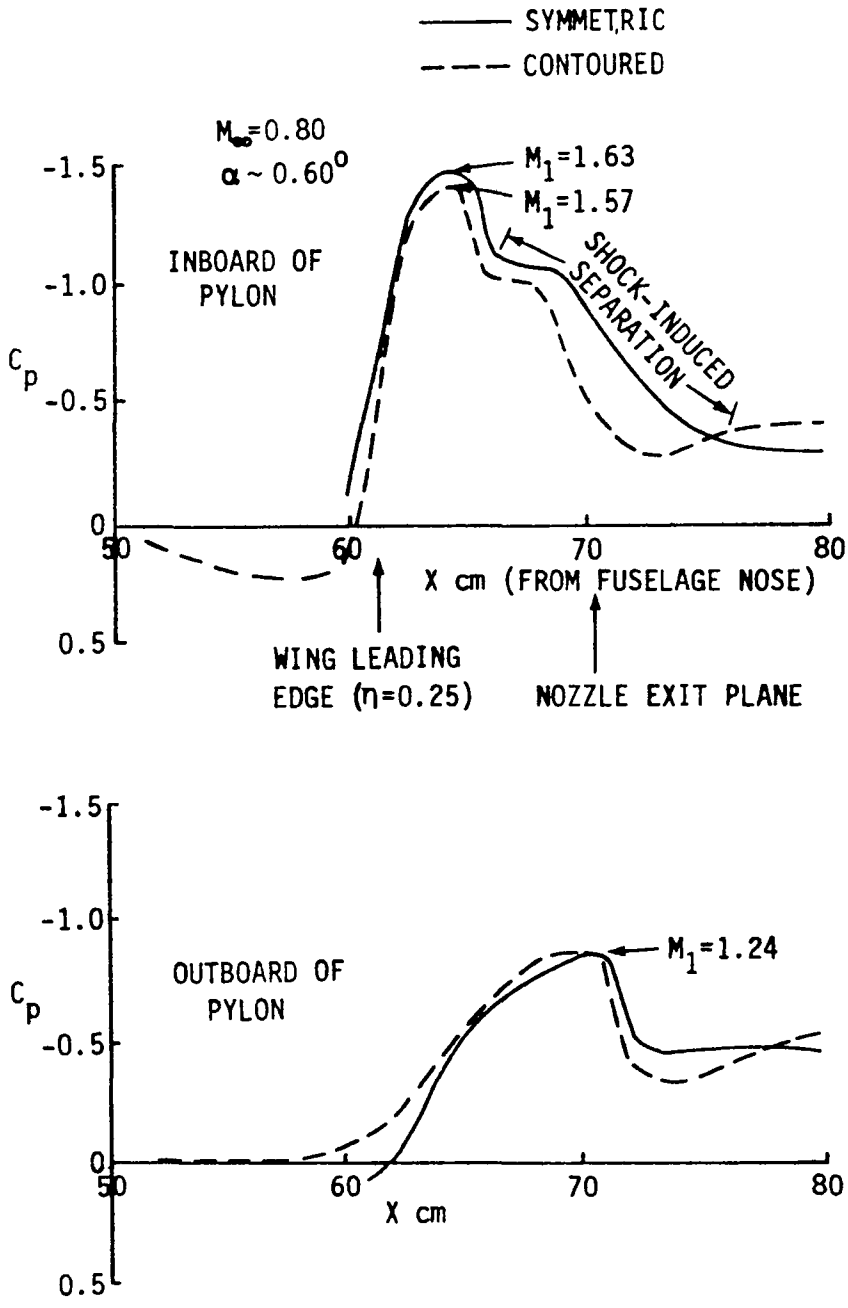

Figure 11 Pylon Pressure Distribution
(M_∞ = 0.80)

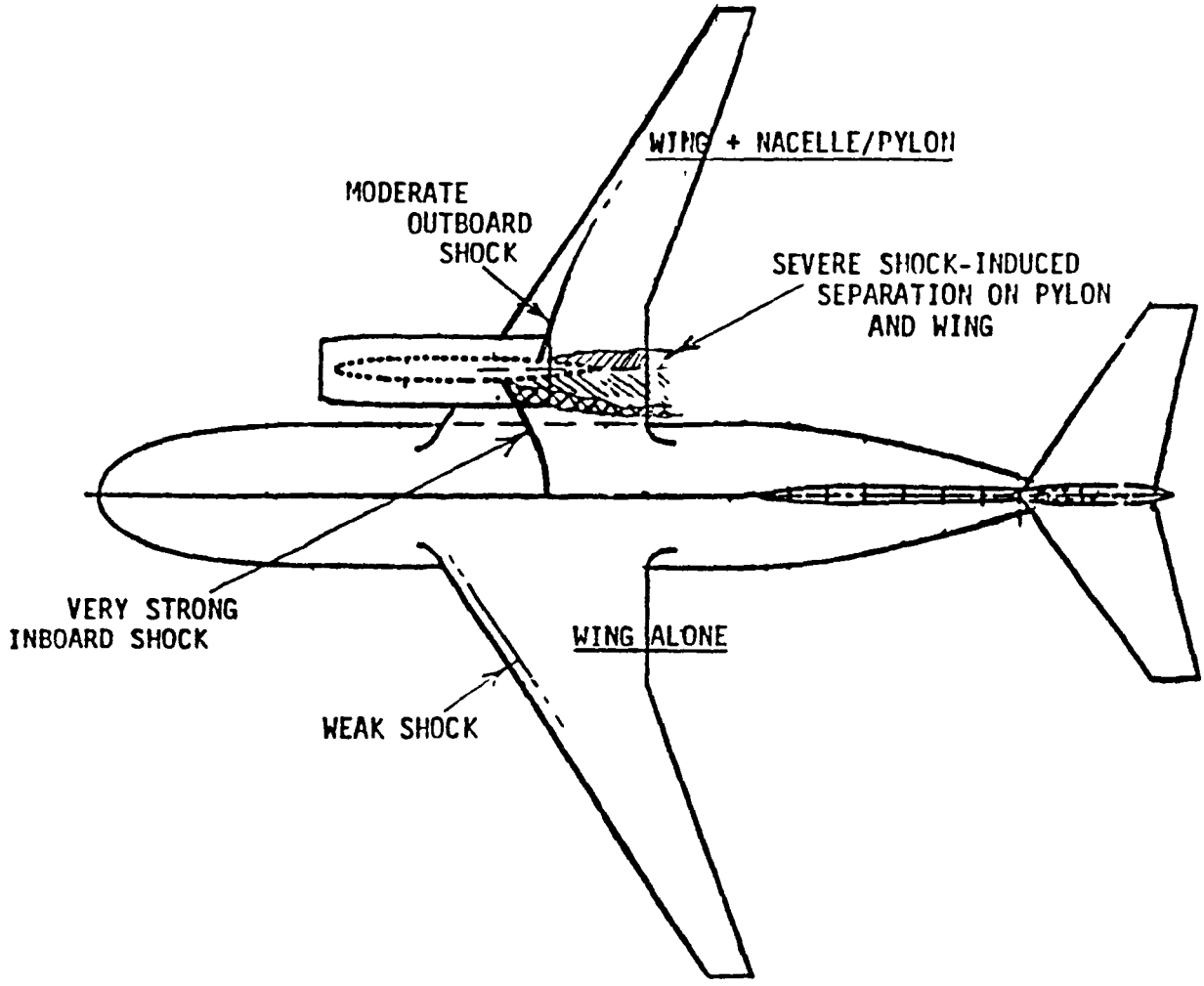

Figure 12 Conjectured Shock and Separation Pattern
($M_\infty = 0.80$)

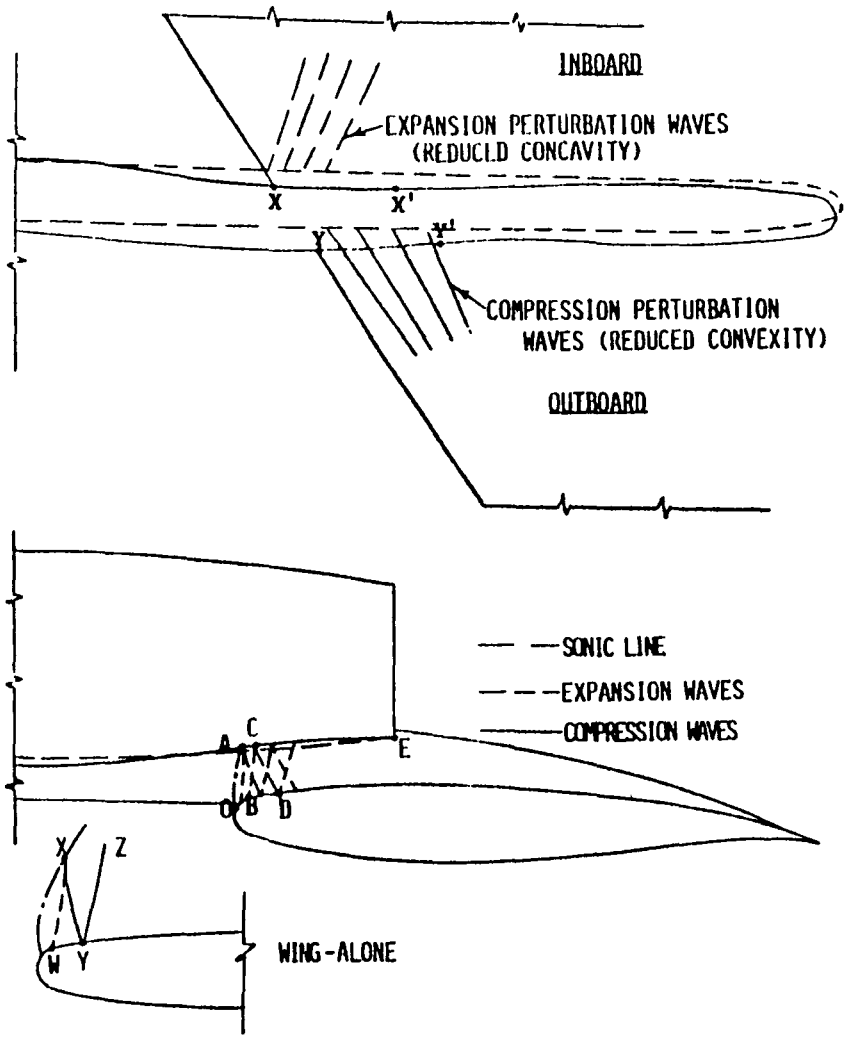

Figure 13 Schematic of the Wave Diagram in the OTW Nacelle/Pylon Configuration ($M_\infty = 0.80$, $C_L = 0.45$)

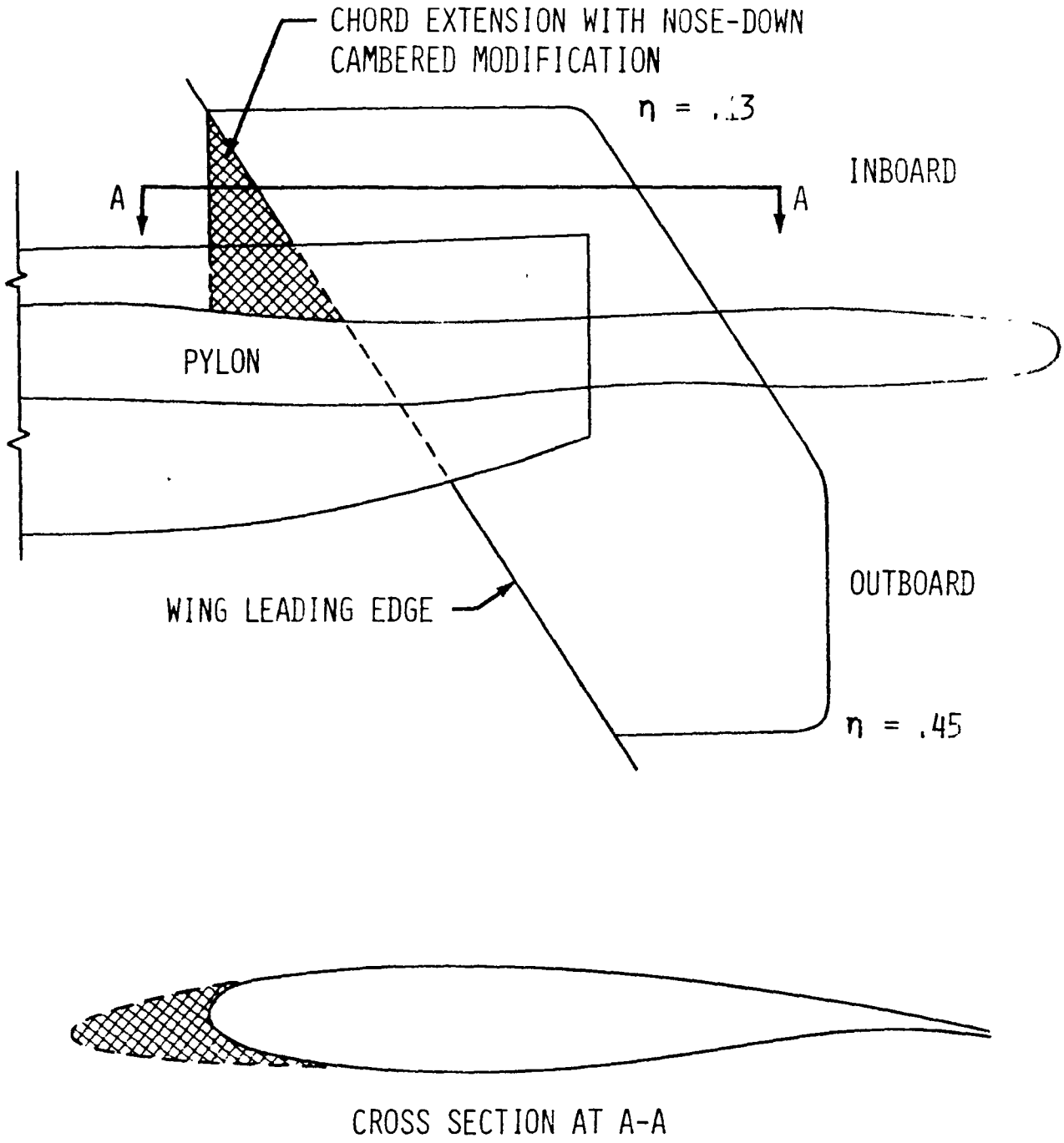

Figure 14 Suggested Configuration Modification - Contoured Configuration

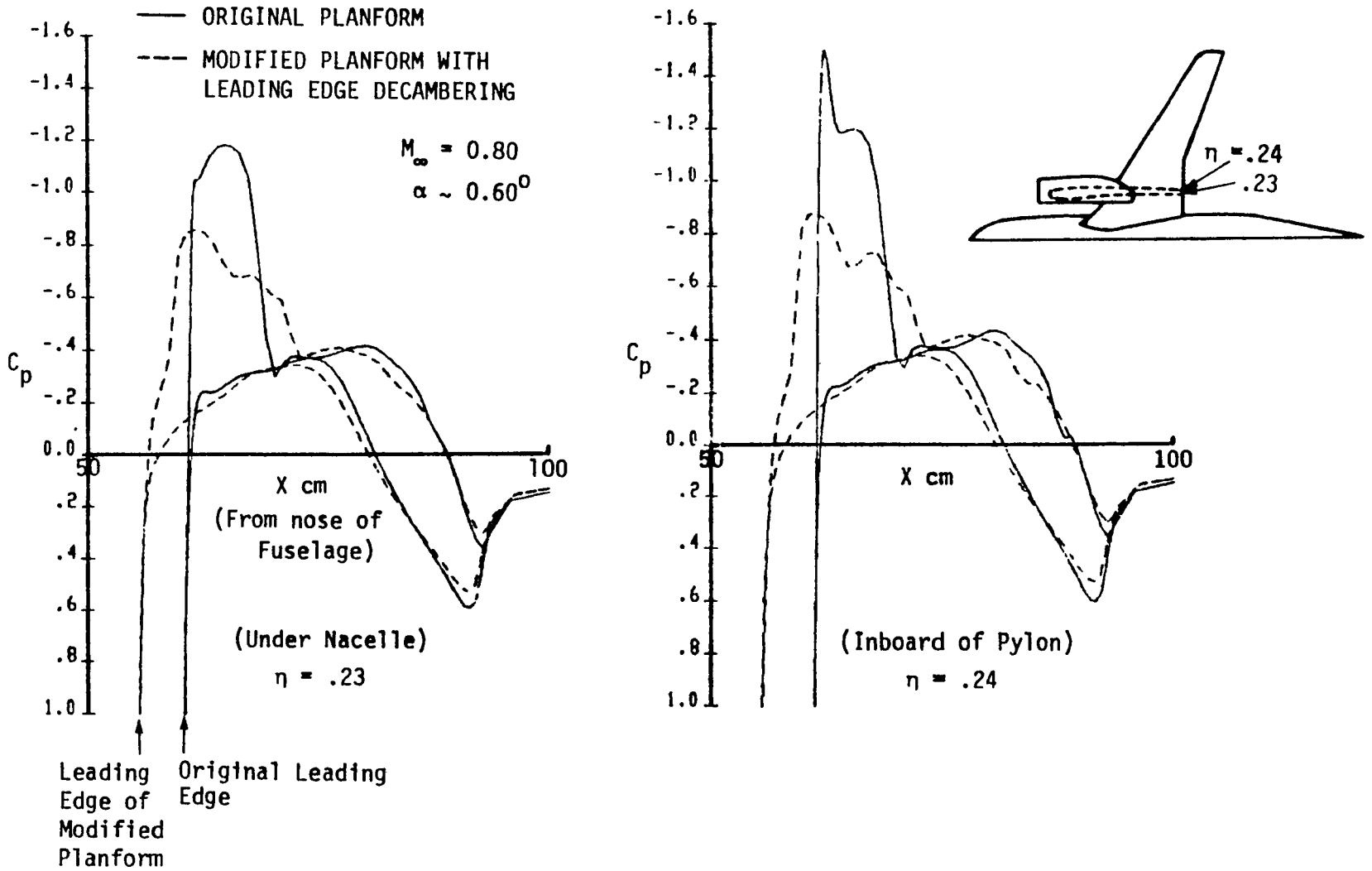

Figure 15 Pressure Distribution of the Over-the-Wing Contoured Nacelle/Pylon Configuration with/without Leading Edge Modification

1 Report No	2 Government Accession No	3 Recipient's Catalog No
NASA CR-165852		

4 Title and Subtitle	5 Report Date
Transonic Perturbation Analysis of Wing-Fuselage - Nacelle-Pylon Configurations with Powered Jet Exhausts	February 1982
	6 Performing Organization Code
7 Author(s)	8 Performing Organization Report No
J. C. Wai, C. C. Sun, and H. Yoshihara	
	10 Work Unit No
9 Performing Organization Name and Address	11 Contract or Grant No
Boeing Military Airplane Company Seattle, WA 98124	NAS1-15887
	13 Type of Report and Period Covered
12 Sponsoring Agency Name and Address	Contractor Report
National Aeronautics and Space Administration Washington, D.C. 20546	14 Sponsoring Agency Code 505-31-43-04

15 Supplementary Notes

Langley Technical Monitor: William K. Abeyounis

16 Abstract

A method using a transonic small disturbance code with successive line over-relaxation (SLOR) is described for treating wing/fuselage configurations with a nacelle/pylon/powered jet. Examples illustrating its use for the NASA transport research model are given. Reasonable test/theory comparisons were obtained.

17 Key Words (Suggested by Author(s))	18 Distribution Statement
Nacelle/pylon Propulsion integration Transonic flow	Unclassified - Unlimited Subject Category 02

19 Security Classif (of this report)	20 Security Classif (of this page)	21 No of Pages	22 Price
Unclassified	Unclassified		

For sale by the National Technical Information Service, Springfield, Virginia 22161

End of Document